Grant agreement No: 325348

LECTURE. Dealing with hydrogen explosions

Compiled by S. Tretsiakova-McNally; reviewed by D. Makarov

Contents

Introduction

The hydrogen economy has become a part of our everyday life. Hydrogen fuelled vehicles are already on our roads. Possible hydrogen explosions can generate high levels of overpressure and thus present threat to life and property. The safety of hydrogen automotive applications and the related infrastructure, including garages, maintenance workshops, parking, and tunnels is one area of concern.

We have already discussed the specific properties and hazards associated with different types of FCH application in previous lectures. This lecture will deal with explosions driven by chemical reaction (i.e. by combustion) and "physical explosions" (i.e. not involving combustion). There are two types of "combustion explosions", i.e. deflagrations and detonations. There are other types of "explosions", e.g. "physical explosions" of vessels by overpressure above the established limit due to overfill (vessel rapture), as a result of runaway reaction, etc. The word "explosion" is rather a jargon one and we will avoid applying it in this lecture where/when possible. Sometimes the use of the term "explosion" could lead to misunderstanding. For example, some standards incorrectly introduce so-called "explosion limit" [1]. This is done in spite of the fact that there can be a significant difference between the "flammability limit", which is relevant for deflagrations, and "detonability limit" [1]. This lecture will introduce First Responders to the phenomena associated with deflagrations and detonations, with their main features and consequences as well as possible means of prevention and mitigation [1]. The most cost-effective and widely used mitigation technique such as vented deflagration will be discussed in detail.

Objectives of the lecture

By the end of this lecture a First Responder/a trainee will be able to:

- Distinguish between deflagrations and detonations
- Recognise the severe consequences of deflagrations and detonations
- Point out the main features of deflagrations and detonations
- Make a distinction between deflagrations in the open and in confined spaces
- Explain deflagration-to-detonation transition (DDT) phenomenon
- Evaluate the effect of blast waves caused by a rupture of a storage tank (in a fire) on people and building structures with the use of nomograms
- Explain the vented deflagration as a main mitigation technique
- Recognise the effects of missiles and debris from explosions
- State the main prevention and suggest possible mitigation measures for explosion events.

Useful terminology

Cell size is the parameter that characterises the detonation sensitivity of a hydrogen-air mixture [2].

Deflagration is the phenomenon of combustion zone propagation at the velocity lower than the speed of sound (sub-sonic) into a fresh, unburned mixture [1].

Detonation is the phenomenon of combustion zone propagating at the velocity higher than the speed of sound (supersonic) in the unreacted mixture [1].

Flame speed is the velocity of the flame with respect to a fixed observer [2].

Overpressure is the pressure in the blast wave above the atmospheric pressure, or the pressure within a containment structure, that is above atmospheric [3].

General features of deflagrations and detonations

Deflagration propagates with the velocity below the speed of sound (sub-sonic) in the unburned mixture, while detonation – with the velocity above the speed of sound (super-sonic). Deflagration front propagates by the diffusion of active radicals and heat from combustion products to unburned flammable mixture. A detonation front is in principle different from a deflagration front. It is a complex of coupled leading shock and following the shock a reaction zone as was for the first time suggested by Chapman (1899) and Jouguet (1905-1906) [1,4,5]. Detonation propagates 2-3 orders of magnitudes faster than deflagration and results in pressures at the detonation front 15-20 times higher than the initial pressure.

Deflagrations in the open, in the absence of any obstacles, could generate overpressures (pressure above the atmospheric one) of about 10 kPa. Deflagrations in the enclosures and/or confined spaces could lead to more significant overpressures. During deflagration the pressure grows practically uniformly within an enclosure. Deflagration in an enclosure can be mitigated by *venting,* the most cost-effective and widespread explosion mitigation technique.

Detonation is a coupled shock and flame front structure, which propagates with a supersonic velocity. The speed of detonation wave depends on the stoichiometry of hydrogen-air mixture and ranges from 1,600 to 2,000 m/s. The overpressures are also much higher: from 1,000 to 1,500 kPa. The venting technique is not applicable to detonations as the pressure arrives to any location and affects a system and/or structural elements simultaneously with the detonation wave, i.e. there is no time to “release” the pressure.

Detonation is the worst case scenario for hydrogen accident. The detonability range of hydrogen in air is from 11 to 59 vol. % [6], which is narrower and within the flammability range of 4-75 vol. %. It is worth noting that the detonability limits are not fundamental characteristics of the mixture as they strongly depend on the size of the experimental set up where they are measured. This will be discussed later in the present lecture.

Deflagrations

The following factors can affect the severity of deflagrations:

- The composition of hydrogen-oxidiser mixture (see Figure 1). Hydrogen-air mixtures close to the maximum burning velocity are more prone to flame acceleration resulting in higher overpressure.
- The uniformity of hydrogen-oxidiser mixture. Non-uniform mixtures have more severe consequences than uniform mixtures with the same initial mass of hydrogen.
- The level of confinement (i.e. walls and ceiling).
- The degree of congestion (the effect of obstacles). The congestion increases turbulence, enhances mixing and increases the rate of combustion.

Dimensionless deflagration pressure for hydrogen-air and hydrogen-oxygen mixtures is shown in Figure 1 [7] as a function of hydrogen mole fraction (volumetric fraction) in a mixture with oxidiser (oxygen or air). The stoichiometric hydrogen-oxygen mixture maximum deflagration pressure in a closed vessel is about 20% greater than the maximum explosion pressure of the stoichiometric hydrogen-air mixture.

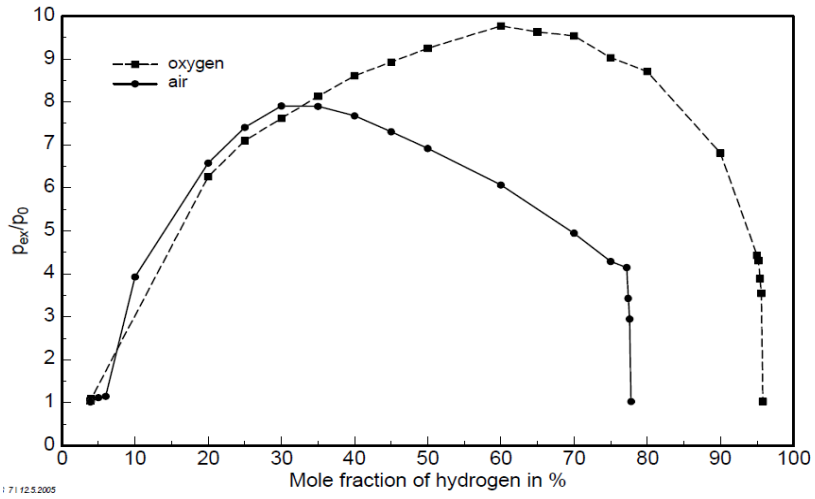

Figure 1. Deflagration pressure of hydrogen-air and hydrogen-oxygen mixtures in a closed vessel at NTP [7].

Hydrogen-air deflagrations in the open atmosphere

A series of experiments with near stoichiometric hydrogen-air deflagrations in unconfined hemi-spherical volumes were performed by Pförtner and Schneider [8] in the Fraunhofer Institute for Fuels and Explosive Materials. The experimental conditions and maximum observed flame speed ($w_{\max}^{\exp}$) are presented in Table 1 for selected tests. The principal aim of these experiments was to investigate the dependence of flame propagation velocity on the hydrogen-air cloud size. Mixtures were ignited at the ground level inside the shell made of thin polyethylene (PE) film to exclude the effect of reflected pressure waves. Burnout of the cloud occurs approximately at two initial diameters that are approximately equal to the cubic root of the products expansion coefficient.

Table 1. Experimental conditions and results for different tests carried out by Pförtner and Schneider [8].

Test No.	Diameter of hemi-sphere D_b, m	Volume of hemi-sphere V, m^3	Hydrogen con centration C, % vol.	Initial temperature T_i, K	Initial pressure p_i, kPa	$S_{ui}^{\exp}$ m/s	$w_{\max}^{\exp}$ m/s
GHT 26	3.06	7.5	29.2	281	99.06	2.32	43
GHT 11	10.00	262	31.0	281	100.66	2.50	60
GHT 34*	20.00	2094	29.7	283	98.93	2.39	84

* - experiments with rhombus-shaped wire net over the hemispherical balloon (in GHT 34 test the rhombus-wire net was laid over balloon and fastened to the ground in 16 points to compensate approximately 7500 N buoyant force).

$S_{ui}^{\exp}$ is the initial burning velocity; $w_{\max}^{\exp}$ is the maximum flame speed.

After burnout the peak deflagration overpressure decays in the form of pressure wave with positive and negative phases. The duration of the positive and the negative phases is independent of the distance for any given size of a balloon. The amplitude of negative pressure peak was usually somewhat larger than that of the positive pressure phase and the negative phase being of shorter duration. Pförtner and Schneider for

spherical sonic waves cited a theoretical result derived by Landau that at any distance the integral of overpressure in time should be equal to zero [8].

Processing of visual images of the flame propagation yielded a continuous increase in flame propagation velocity up to a maximum value, which was reached at a distance between the initial radius of the cloud R_{hsph} and 1.5 R_{hsph}. For initially quiescent stoichiometric hydrogen-air mixture this upper limit was estimated as 125 m/s with a peak overpressure 13 kPa [8]. The experimental results indicate that the flame propagation velocity approaches the upper limit with the increase of the cloud size.

In test GHT 34 corresponding to 29.7 vol. % hydrogen in its mixture with air in a 20 m diameter hemisphere, the maximum flame propagation velocity was 84 m/s with the initial burning velocity estimated in [8] as 2.39 m/s (the expansion coefficient of combustion products was calculated as 7.26 with a density of combustible mixture 0.8775 kg/m^3 and a speed of sound 397.3 m/s). Errors in velocity measurements were assessed as ±5% without taking into account certain asymmetries in flame propagation.

In order to make the hydrogen-air flame visible in daylight finely ground sodium chloride (NaCl) powder was dispersed inside the balloon at the end of filling process to produce a yellow-coloured flame. Generally 10 to 12 piezo-resistive Kistler pressure sensors (100 kPa range, natural frequency 14 kHz) were used. These were mounted in a steel case having a mass of 20 kg in a way that their pressure-sensitive surfaces were fitted flush with the surface of the ground and covered with a 2 mm thick layer of silicone grease on the membrane to avoid the influence of temperature and heat radiation. In addition, a sensor located at 5-m distance from the ignition source was protected with a laminated plastic plate screwed to the steel casing and having an opening of 4 mm diameter in the middle. For the GHT 34 test an additional pressure sensor was installed at a right angles to the axis with main sensors and mounted on a vertical timber wall 1x1 m^2 (head-on measurement).

The deflagration pressure was measured at distances 2.0, 3.5, 5.0, 6.5, 8.0, 18, 25, 35, 60, and 80 m from the initiation point. The mixture was ignited by pyrotechnical charges with total ignition energy 150 J. The pressure transients of sensors inside the combustion products did not return to zero after the negative pressure phase, except for the sensor installed at 5 m. This can be attributed to the fact that the transducers were thermalized to high temperatures during the explosion. Since they did not remain at the temperature at which they were calibrated, they were no longer calibrated and did not return to the baseline. This is an indication that the protective measures taken by the experimentalists to insulate these transducers were insufficient for this large test.

Figure 2 shows that the flame propagated in an almost hemi-spherical form. The balloon shell first stretched slightly outwards until it burst when the flame had reached about half of the original radius of the balloon 0.5R_0.

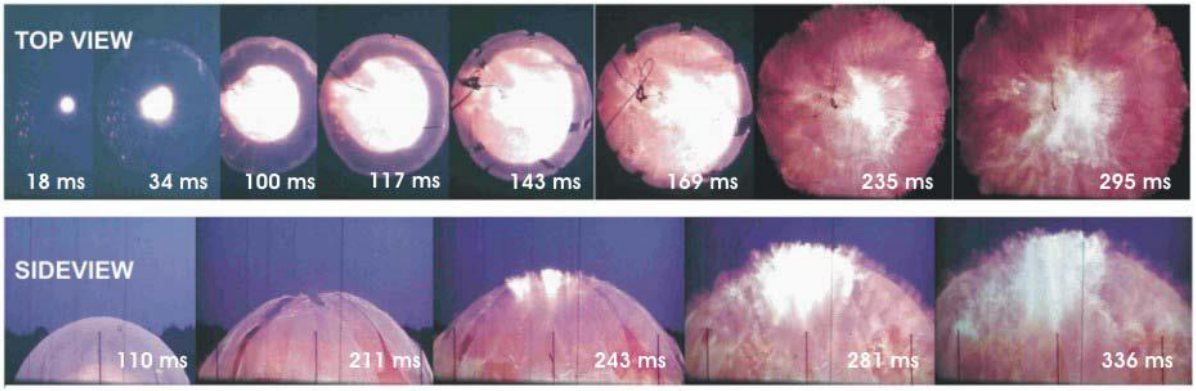

Figure 2. The snapshots of test GHT 34 in a 20 m diameter hemisphere [1,8,9].

The explosion overpressure of about 6 kPa was practically the same within the cloud distances in GHT 34 test. A sharp overpressure peak Δp_F of about 10 kPa in the pressure transients followed the flame propagation. It could be an effect of a high temperature, gas dynamics effect, or it can be assumed that as the flame passed the pressure sensor, it ignited the gas in the space between the laminated plastic plate with 4 mm diameter orifice and the sensor, so that a partially confined explosion occurs causing the peak pressure Δp_F, similar to pressure peak generation in a vented vessel (mentioned above laminated plastic plates with 4 mm diameter opening could be considered as a vessel wall with a vent).

For hydrogen-air deflagration (test GHT 11) in 10.0 m diameter hemisphere the comparison between experiment and simulations was carried out by Molkov et al. (2007) [10]. Pressure dynamics recorded at 6.85, 8.79, and 10.8 m from the ignition source are presented in Figure 3.

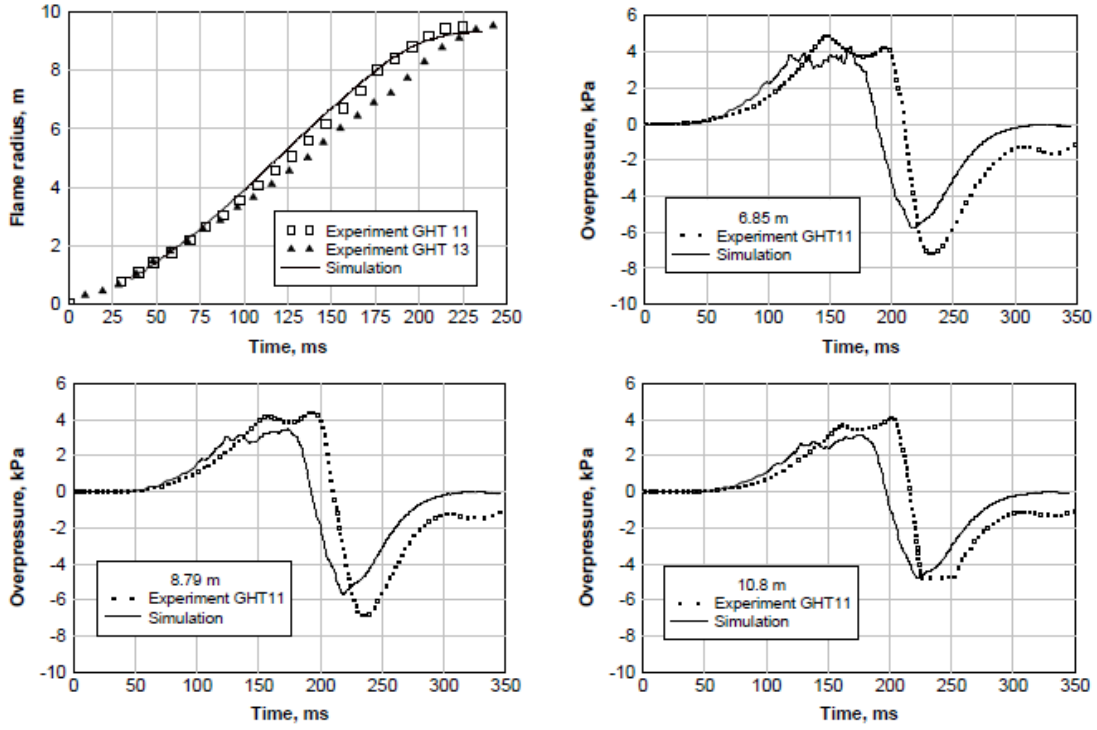

Figure 3. A comparison between the experiment (GHT 11) and simulation for hemispherical balloon of 10.0 m in diameter: radius of leading edge of a flame front (top left); pressure dynamics at different distances from the ignition source - 6.85 m (top right), 8.79 m (bottom left), 10.8 m (bottom right).

Gaseous deflagrations in the open atmosphere generate outgoing pressure waves. The acoustic theory can be applied for deflagration generated pressure waves. Pressure in a blast wave can be estimated as [11] shown below:

$$\frac{p(t,R_w)-p_i}{p_i}=\frac{\gamma(E_i-1)}{\left[1+r_b(t)/c_0t\right]E_ic_0^2}\frac{r_b(t)}{R_w}\left[2w^2+r_b(t)\frac{dw}{dt}\right] \quad (1)$$

where $r_b(t)$ is the flame radius at moment t, m; R_w is the distance at which pressure p is estimated, m; c_0 is the speed of sound, m/s; w is the flame front propagation velocity, m/s. The key conclusion from this formula is that the pressure wave peak depends on both the flame propagation velocity and the flame acceleration, especially at large radii. Deceleration of the flame front results in a pressure drop in the pressure wave. This formula states as well that the pressure wave decays inversely proportional to the distance from the ignition source [1].

Deflagrations in a closed vessel

Hydrogen safety engineering requires prediction of pressure loads for realistic scenarios, which always include a formation and a consequent combustion of a non-uniform flammable mixture [1]. The Large Eddy Simulations (LES) model has been developed to reproduce dynamics of lean uniform and non-uniform (gradient) hydrogen-air premixed combustion and validated against a large-scale experiment in a cylindrical vessel (5.7 m height and 1.5 m diameter) [12, 13].

The experiments: an overview

The experiments were carried out in a hermetically sealed 5.7 m height and 1.5 m internal diameter cylindrical vessel. All experiments were performed with dry hydrogen-air mixtures at 25±3 °C. The ignition source was located 15 cm beneath the top of the vessel. Several fine-wire (75 micron diameter) thermocouples were located on both sides along the vessel's axis to detect the flame position in the vessel. The thermocouples were spaced 0.55 m apart, vertically, in a plane passing through the axis. Several piezoelectric transducers were installed at different intervals along the axis of the cylinder.

For uniform hydrogen-air mixtures, three fans were used to homogenise the mixture. For uniform hydrogen-air mixtures containing 12.8, 14, 16, and 20 vol. % of hydrogen the data on flame propagations along the cylinder axis are only available [14].

To establish concentration gradients, hydrogen and air were first pre-mixed in a small chamber prior to entering the top of the cylinder, then hydrogen was introduced continually by increasing hydrogen concentration in the vessel. The rate of hydrogen increase was pre-determined on the test-by-test basis to create the desired gradient. After the concentration gradient was established, hydrogen concentrations were measured at the vertical sampling locations [15]. For a non-uniform mixture with 12.6 vol. % average concentration the hydrogen distribution along the vessel axis is reported in [15]: 27 vol. % at the top of the vessel, and decaying to 2.5 vol. % at the bottom. Pressure dynamics and flame propagation in the 12.6 vol. % gradient hydrogen-air mixture were compared with those in a well-mixed uniform 12.8 vol. % mixture containing equivalent amount of hydrogen [15].

Effect of hydrogen concentration and concentration gradient on dynamics of deflagrations Figure 4 shows experimental flame propagation dynamics from igniter downward along the vessel centre-line [15] in comparison with simulation results [13]. Increase of hydrogen concentration in 1.6 times (from 12.8 vol. % to 20 vol. %) results in 7 times faster flame propagation.

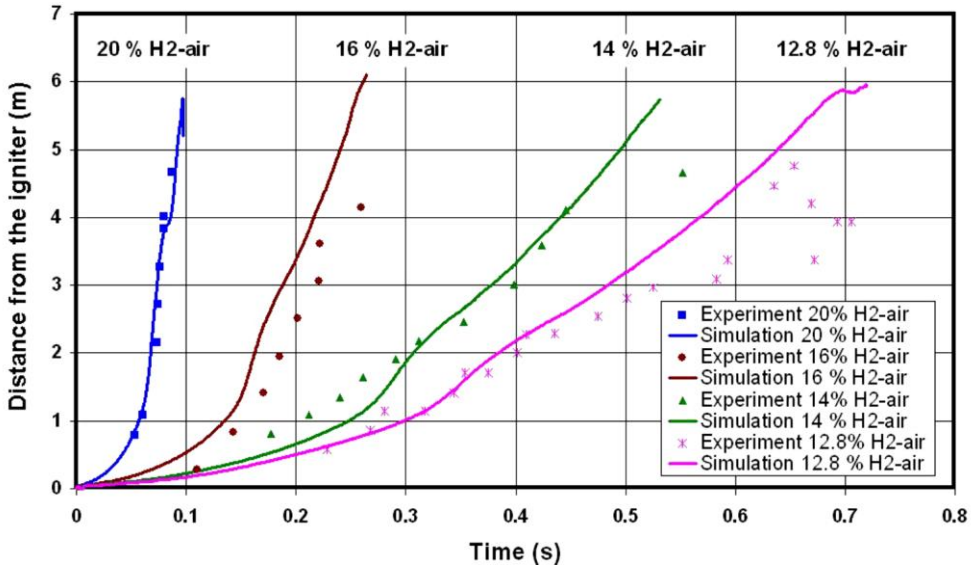

Figure 4. The experimental and simulated flame propagation dynamics along the vessel axis for 20, 16, 14, and 12.8 vol. % hydrogen-air mixtures [13].

Combustion instabilities, including preferential-diffusive-thermal and hydrodynamic ones, cause perturbations of the laminar flame, triggering a formation of a *cellular flame structure* and then *flame wrinkling* [16-21].

The *selective diffusion* is one of phenomena which destabilises flat laminar flame front, pronounced for lean hydrogen-air mixtures, and thus drastically affects deflagration dynamics of lean mixtures. Due to selective diffusion protruded (convex) into unburned mixture wrinkles propagate with higher velocity compared to concave wrinkles due to the redistribution of hydrogen close to these wrinkles. Indeed, due to a higher diffusivity of hydrogen its concentration at convex wrinkles will grow and at concave wrinkles will decrease. This will lead to an increase of wrinkles amplitude. This mechanism results in increase of burning rate, which for external observer looks like increase of burning velocity. The lower hydrogen concentration the more pronounced this mechanism, leading to easier acceleration and turbulisation of initially laminar flames (though the turbulent burning velocity for leaner mixture will be always lower under the same conditions).

The selective diffusion effect depends on wrinkle curvature, i.e. reciprocal to radius [1]. There is a curvature of wrinkle, at which the effect of selective diffusion on mass burning rate is at its maximum. Because a real flame has a spectrum of wrinkles of different curvature, the flame will be led by those wrinkles that have this optimum from a point of view of maximum burning rate curvature. These wrinkles will be responsible for the propagation of a leading edge of flame front and called "*leading points*". An increase in the flame speed results from the development of the cellular structure in combination with formation of leading flamelet structures, i.e. leading points [18, 19, 22]. Kuznetsov and Sabelnikov [22] stated that the turbulent flame speed is controlled by the burning velocity of these leading point flamelets, where the mixture composition is locally altered due to different diffusivity of fuel and oxidiser, i.e. *preferential diffusion.*

To account for preferential diffusion effects for curved hydrogen flames the leading point concept was applied in the LES model [13]. Figure 5 shows the augmentation of burning velocity by the leading point phenomenon, χ_{lp}. Lean mixtures are all affected by this mechanism. For example, for 10 vol. % hydrogen-air mixture the laminar burning velocity has to be multiplied by the factor 2.4.

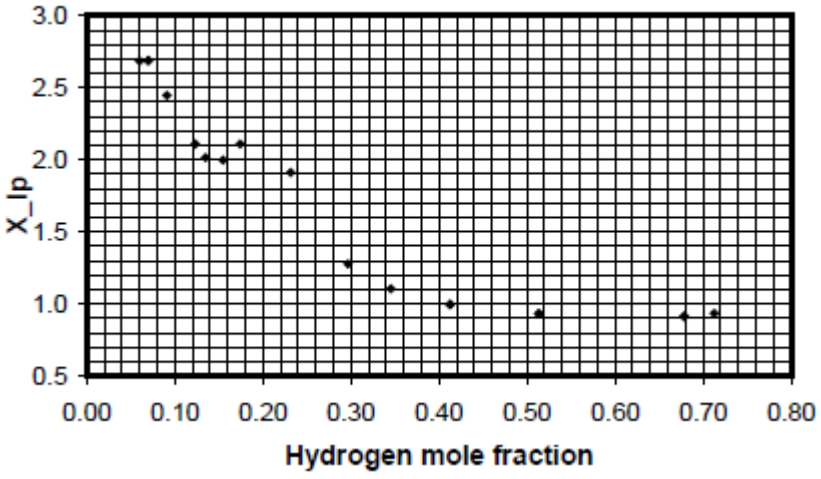

Figure 5. Leading point wrinkling factor as a function to hydrogen mole fraction [13].

The preferential diffusion effect coupled with flame curvature is pronounced for lean hydrogen-air mixtures and has to be accounted for in the premixed combustion model to predict deflagration dynamics and pressure build-up.

The effect of leading point mechanism on prediction of deflagration dynamics in lean hydrogen-air mixtures is shown in Figure 6 using simulation [13] of the same closed vessel deflagration experiment [15]. Without the implementation of leading point factor into the turbulent burning velocity model, the flame propagation

is significantly underestimated compared to the experimental data. Indeed, for 20 vol. % hydrogen-air mixture the flame propagation velocity is equal to 44 m/s at distance 1 m from the ignition source and 162 m/s at distance 3 m with the turbulent burning velocity corrected by the leading point factor, and it is only 22 m/s and 50 m/s at 1 m and 3 m respectively without the correction. In the case of uniform 12.8% vol. hydrogen-air mixture, the flame speed is 7.7 m/s at 1 m with correction and only 2.95 m/s without correction [1].

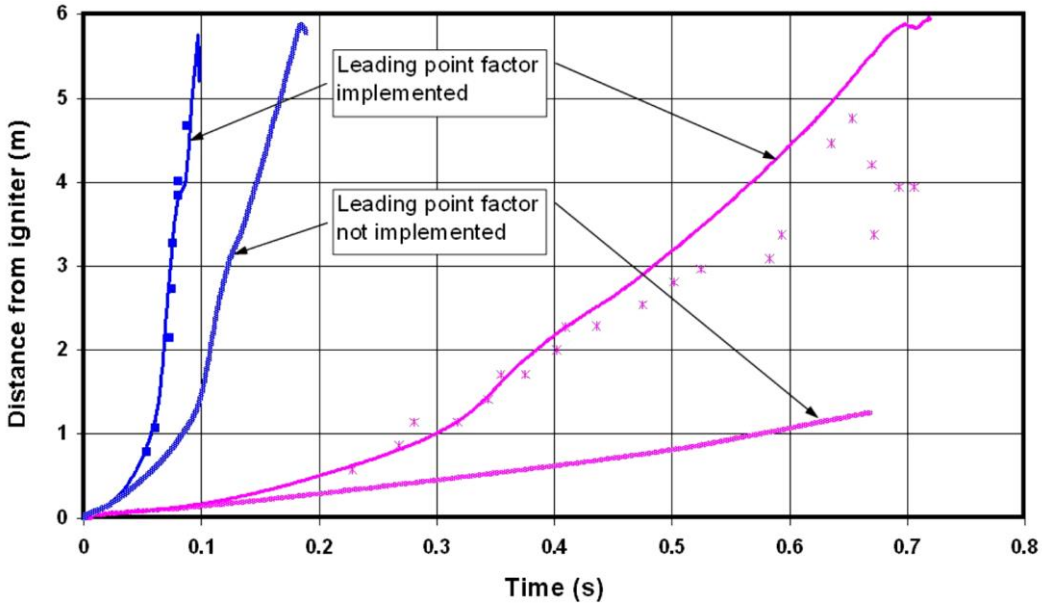

Figure 6. The experimental and simulated flame propagation with/without implementation of the leading point correction for uniform 12.8 vol. % and 20 vol. % hydrogen-air mixtures.

Figure 7 compares flame propagation dynamics for the uniform (12.8 vol. %) and the gradient (average 12.6 vol. %) hydrogen-air mixtures. For a scenario with practically the same amount of hydrogen released, flame propagates much faster in the mixture with the concentration gradient. This can be explained by the higher hydrogen concentration at a location of the ignition source, i.e. 27 vol. % hydrogen, which is close to the stoichiometric composition. It can be estimated that for the gradient hydrogen-air mixture the flame speed reaches 57 m/s and 209 m/s at 1 m and 3 m from the ignition source respectively. For the uniform 12.8 vol. % hydrogen-air mixture the flame speed at the same locations reaches only 7.7 m/s and 9 m/s, respectively [1].

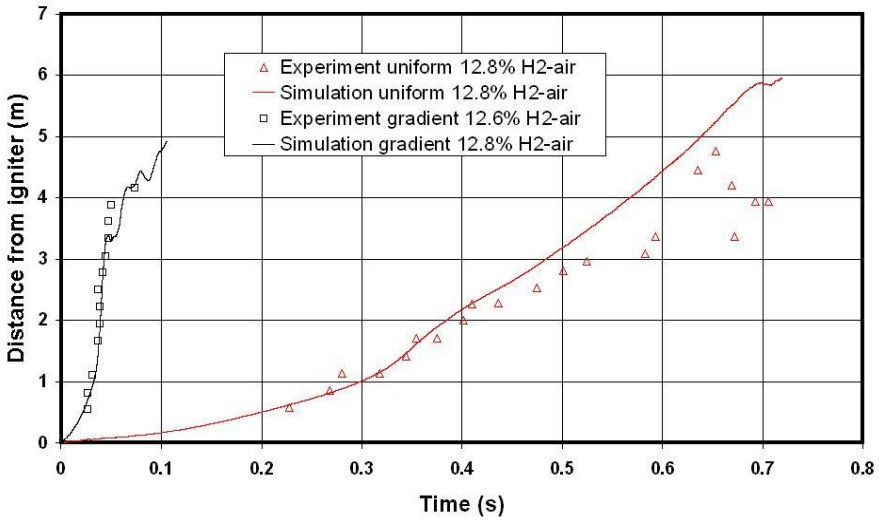

Figure 7. The experimental and simulated flame propagation for 12.8 vol. % uniform hydrogen-air mixture and for 12.6 vol. % (averaged) gradient hydrogen-air mixture.

A comparison of experimental and simulated pressure dynamics for 12.8 vol. % uniform hydrogen-air mixture and for 12.6 vol. % gradient hydrogen-air mixture is shown in Figure 8. The pressure rise is much steeper in the mixture with the hydrogen concentration gradient compared to the uniform 12.8 vol. % hydrogen-air mixture. This is consistent with flame speeds observed for deflagrations with top ignition both in experimental study by Whitehouse et al. [15] and simulations [13]: mixtures with hydrogen concentration gradient have much shorter times to peak overpressure than uniform mixtures with the same quantity of hydrogen because of higher hydrogen concentration at the ignition point [1].

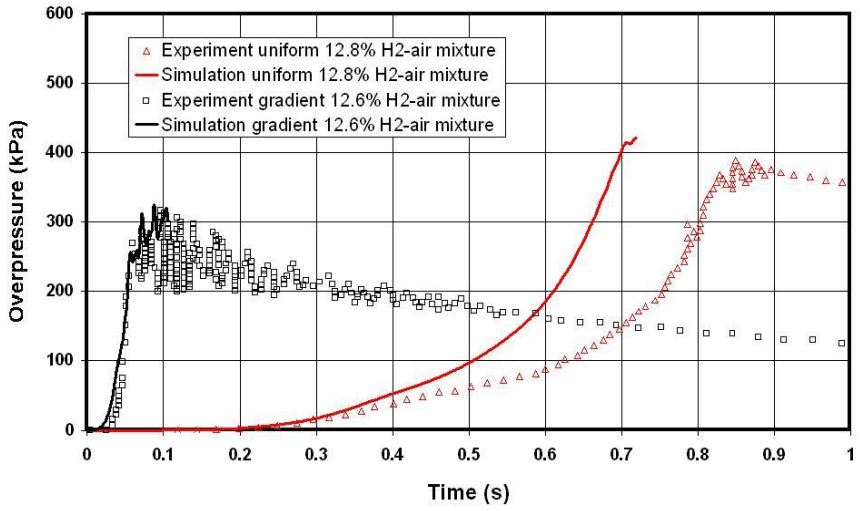

Figure 8. The experimental and simulated pressure dynamics for uniform 12.8 vol. % hydrogen-air mixture and non-uniform (12.6 vol. % averaged) gradient hydrogen-air mixture.

Thus, the simulated pressure for non-uniform mixture is close to the one measured in the experiment. Contrary, simulated pressure develops faster than experimental pressure transients for the uniform mixture. This can be explained by absence of heat losses from hot combustion products to walls in the simulations. Heat losses have to grow with time [1].

Hydrogen-air deflagrations in a tunnel

A typical amount of on-board stored hydrogen in a passenger car is about 6 kg and in a bus is up to 40 kg. The release of several kilograms of hydrogen from a hydrogen-powered vehicle during an accident in a tunnel, followed by an ignition and thus deflagration, is a possible accident scenario.

Large-scale experiments on hydrogen-air deflagrations in a 1/5th real scale tunnel were performed by Groethe et al. [23] and later on simulated by Molkov et al. [24]. The experimentalists reported on pressure and impulse (i.e. the time integral of pressure) generated by such deflagrations, while the simulations enabled the analysis of phenomena, which were not reported in the experimental study, e.g. a significant increase in the maximum explosion overpressure in the vicinity of the obstacles due to the obstacle side-on pressure wave reflection in later stages of the event. The latter has practical safety implications: a recent numerical study by Gamezo et al. [25] of the deflagration-to-detonation transition (DDT) in an obstructed small-scale tube containing a hydrogen-air mixture demonstrated that the reflection of a developing shock on repeated obstacles is a reason for shock-to-detonation transition [25].

The experiment overview

The scaled tunnel was 78.5 m in length, 1.84 m in height, with a horseshoe shape cross sectional area of 3.74 m^2. Uniform hydrogen-air mixtures containing 20 vol. % and 30 vol. % of hydrogen with a total volume of 37.4 m^3 volume (10 m long cloud) were prepared in the middle of the unobstructed tunnel and ignited at the

centre of the tunnel at floor level. The amount of hydrogen for the near stoichiometric (30 vol. %) hydrogen-air cloud was equal to 1 kg. An additional experiment with obstructions was carried out only for a 30 vol. % hydrogen-air mixture. Mock vehicles with the size LxWxH=940x362x343 mm were used as the obstacles. The distance between the vehicles was equal to a "vehicle" length. A blockage ratio (BR) for this type of obstacle was 0.03.

Experimental and simulated results

A comparison between the maximum experimental and simulated overpressures along the tunnel is presented in Figure 9 for all three experiments. Side-on obstacle overpressure is available for numerical simulations only. There is a good agreement for all cases with an insignificant under-prediction of the maximum overpressures in simulations. This result is very positive for the LES model validation bearing in mind that the model was "calibrated" for very different conditions of unconfined deflagrations.

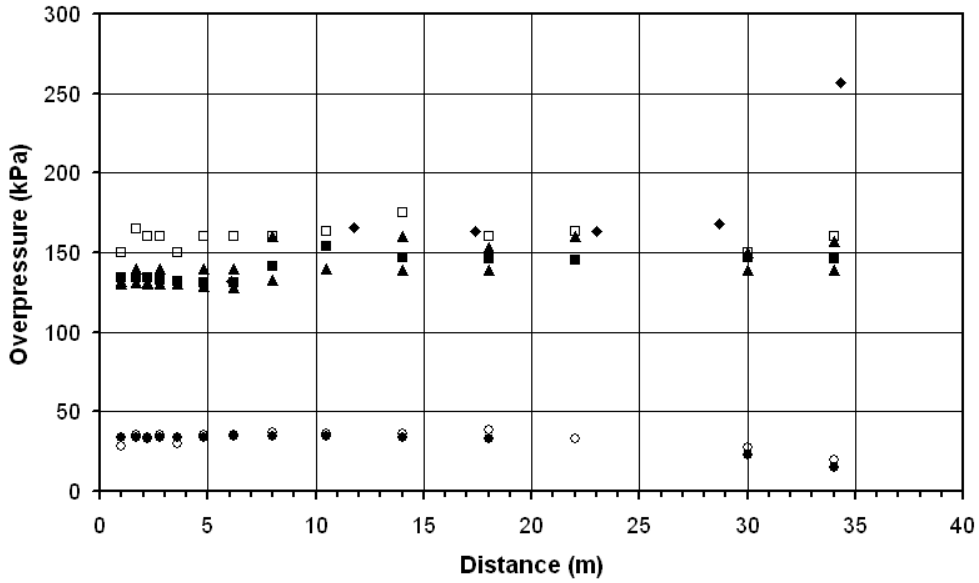

Figure 9. Maximum deflagration overpressures along the tunnel (distance is given from the tunnel centre): 20 vol. % hydrogen-air mixture (○ – experiment; ● – simulations); 30 vol. % hydrogen-air mixture, unobstructed tunnel (Δ - experiment; ▲- simulations); 30 vol. % hydrogen-air mixture, obstructed tunnel (□ – experiment; ■ – simulations, ceiling; ◆- simulations, obstacle).

The LES analysis for the cases without and with obstructions inside the tunnel demonstrated significantly higher deflagration-generated overpressure on the obstacle surfaces (◆in Figure 9) compared to the overpressure measured at the ceiling level (■ in Figure 9). Indeed, in the agreement with experimental data the maximum overpressures simulated above the obstacle level are practically the same as those measured experimentally for the cases with and without obstacles. However, with the increasing distance from the ignition source, the difference between static side-on obstacle overpressure and the static overpressure on the ceiling increase. This is an indication that the initial pressure wave from combustion forms a shock, which reflects from the rigid "vehicle" surface, thus increasing the static pressure at the stagnation area [1].

The pressure in the reflected shock, p_3, can be estimated from the values of the initial pressure, p_1, and the incident shock, p_2, using the following formula [26]:

$$\frac{p_3}{p_2} = \frac{(3\gamma-1)p_2-(\gamma-1)p_1}{(\gamma-1)p_2+(\gamma+1)p_1} \quad (2)$$

For a specific heat ratio of γ=1.4, p_1=1 bar and p_2=2.5 bar the ratio is about p_3/p_2=2.2. Because the formation of the shock is not yet finished and the reflection is not exactly normal the simulated ratio is lower than theoretical and only about p_3/p_2=1.5.

The simulated shock wave structure at a distance of 34 m from the ignition source reproduced transient pressures and impulse quite close to those measured in the experiments (Figure 10). The simulated arrival time of the shock practically coincides with the experimental value. Somewhat faster arrival times of simulated pressure waves can be observed in Figure 10. This could be explained by the higher speed of sound in the combustion products in the simulations. Indeed, the model does not include heat losses from combustion products. This would reduce the temperature and hence the speed of sound [1].

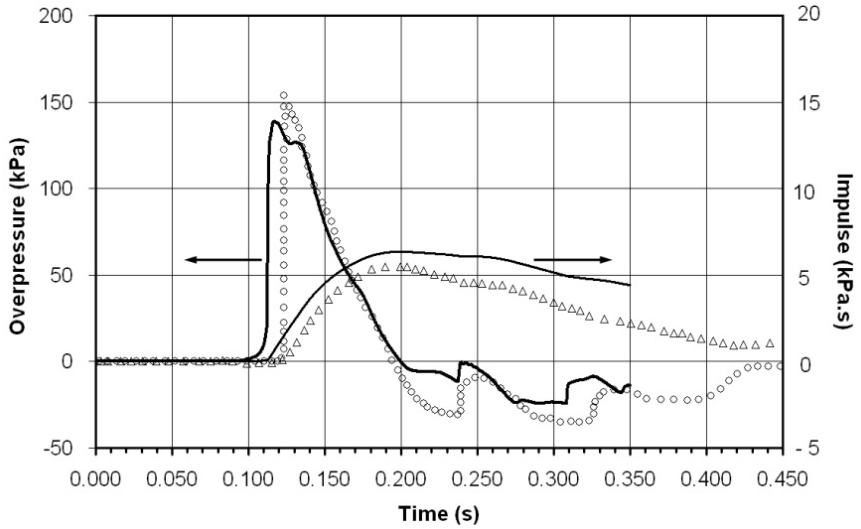

Figure 10. A comparison between the experimental and simulated pressure dynamics and impulses at a distance of 34 m from the ignition source: experimental pressure dynamics (circles) and impulse (triangles), simulated pressure dynamics and impulse (solid lines) [1].

Figure 11 shows the simulated pressure dynamics at different distances from the ignition source along the tunnel. The formation of the shock wave with a steep leading edge from the initial sloping shape pressure wave during deflagration progression can be seen. The maximum overpressure is practically the same along the tunnel. Bearing in mind a level of overpressure observed in the experiments and reproduced in simulations, a serious damage to life and property inside the tunnel can be expected for the considered scenario for the whole length of a tunnel as a shock wave does not indicate the tendency to decay with distance [1].

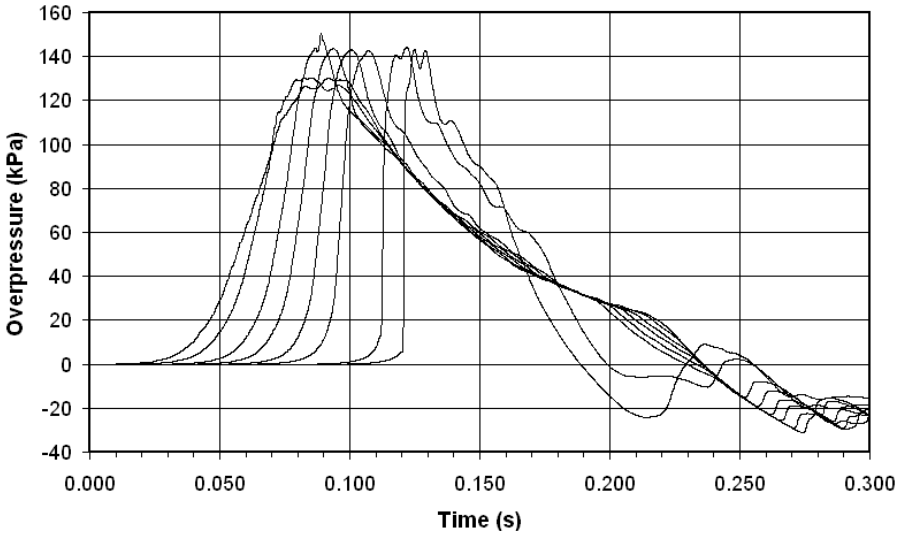

Figure 11. The formation of the shock wave during pressure wave propagation along the tunnel (ceiling level). Simulated pressure transients at distances 2.8, 6.2, 10.5, 14, 18, 22, 30, and 34 m from the ignition source.

The difference in the dynamics of the overpressure at a ceiling level and side-on obstacle overpressure along the tunnel is shown in Figure 12. The shock is formed at the end of the tunnel. Pressure transients have similar dynamics at various locations along the tunnel cross section. An exception is a part of the pressure-time curve close to the maximum overpressure, which is affected by the absence (ceiling) or presence (obstacle's side) of the blast wave reflection. There is no experimental data available on the flame propagation inside the tunnel. There are distinctive phases of the leading edge of the flame front acceleration and deceleration in simulations (Figure 12). The flame front reaches the end of the right part of the tunnel about 270 ms after ignition [1].

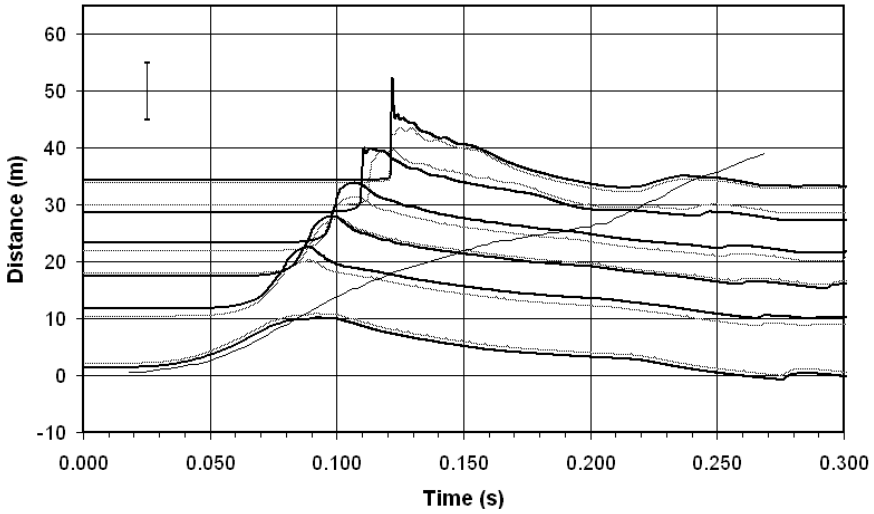

Figure 12. Simulated static overpressure dynamics (dotted (gray) lines – ceiling overpressures; solid lines – side-on obstacle overpressures; location of the computational pressure gauges can be read from the ordinate axis) and flame propagation dynamics (position of flame on tunnel's centre line in time) [1].

In order to understand the dynamics of the deflagration in the tunnel in more detail the simulation results have been analysed. This analysis is presented in Figure 13 (left), along with data on hydrogen concentration in air which is presented in Figure 13 (right).

Computational visualization of the overpressure field in the tunnel, overlapped with locations of the turbulent flame front brush (c=0.1-0.9), for a series of consequent moments is shown in Figure 13 (left). This confirms the flame acceleration at initial stage, then deceleration and acceleration again up to almost the moment when the flame front exits the tunnel approximately 270 ms after ignition. The formation of the shock with time is clearly seen. Areas of high side-on obstacle pressure can be identified. The shock leaves the tunnel at approximately 131 ms, at this time the flame has only passed half way along the tunnel. The rarefaction wave is seen in Figure 13 (left), this propagates inside the tunnel after the shock wave leaves the tunnel. This wave, and the resulting flow induced, is responsible for the second acceleration of the flame.

Figure 13 (right) shows the movement of the flammable hydrogen-air mixture in a range of concentrations relative to the flame position; from the initial concentration of 30 vol. % down to the lower flammability limit of 4 vol. % of hydrogen in air. The dilution with time of the initially uniform near stoichiometric 30 vol. % hydrogen-air mixture (black colour in Figure 13, right) by the air at the contact surface is seen. There is an essential decrease in the volume of flammable mixture present at approximately 140 ms. The flammable cloud at this time is above the level of the obstacles. Slow combustion of the hydrogen-air mixture with concentrations close to the lower flammability limit continues up to t=350 ms. After 140 ms combustion no longer has a significant effect on the flow dynamics, to the contrary the flow induced by the pressure waves is responsible for the second flame "acceleration" and the reverse movement of the flame back to the centre of the tunnel after 290 ms.

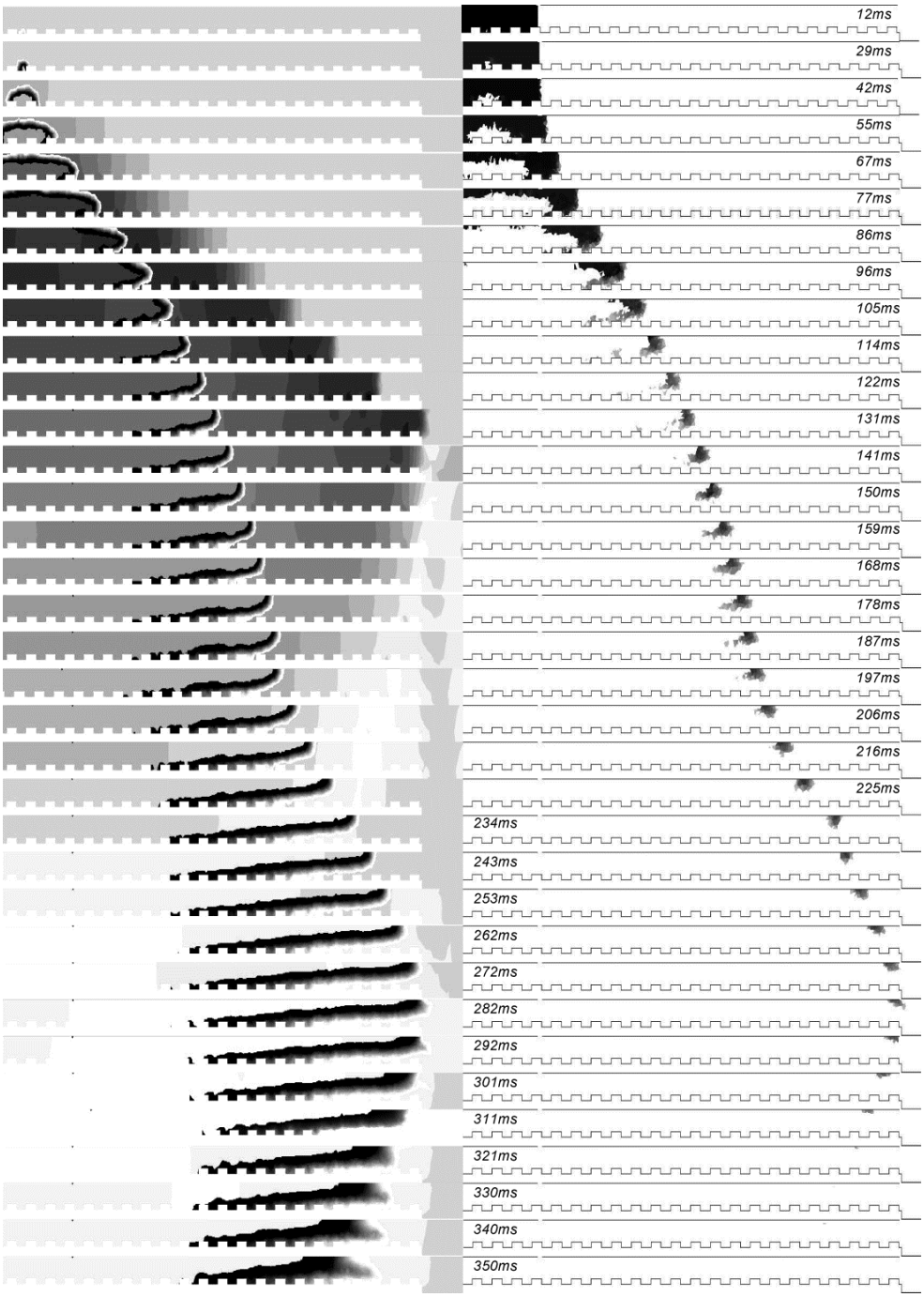

Figure 13. Left: pressure and rarefaction waves, flame front (c=0.1-0.9, t<270 ms), and combustion products (c=0.1-0.9, t>270 ms). Right: flammable hydrogen-air mixture propagation in the tunnel (black colour refers to 30 vol. % of hydrogen in air, grey colour corresponds to 4 vol. % of hydrogen). Time after ignition refers to both columns [1].

From the analysis of Figure 13 (left and right) it follows that approximately 140 ms after ignition the premixed combustion proceeds in the upper part of the tunnel above the obstacles and a large mixing layer of combustion products and air develops. This can assist in the assessment of a thermal hazard inside the tunnel.

From Figure 12 it is seen that the deceleration of flame is started at approximately 80-90 ms. There can be two main reasons for the flame deceleration. The first is a reduction in the transient total flame front area and the second is a decrease in the laminar burning velocity in the flamelets. Indeed, at approximately 85 ms the flame reached the ceiling and the flame surface area begins to reduce.

The pressure transients at two locations at the end of the tunnel and two just outside the tunnel are shown in Figure 14. The pressure drops quite fast to achieve a value of approximately 5 kPa at a distance approximately 1 diameter outside the tunnel.

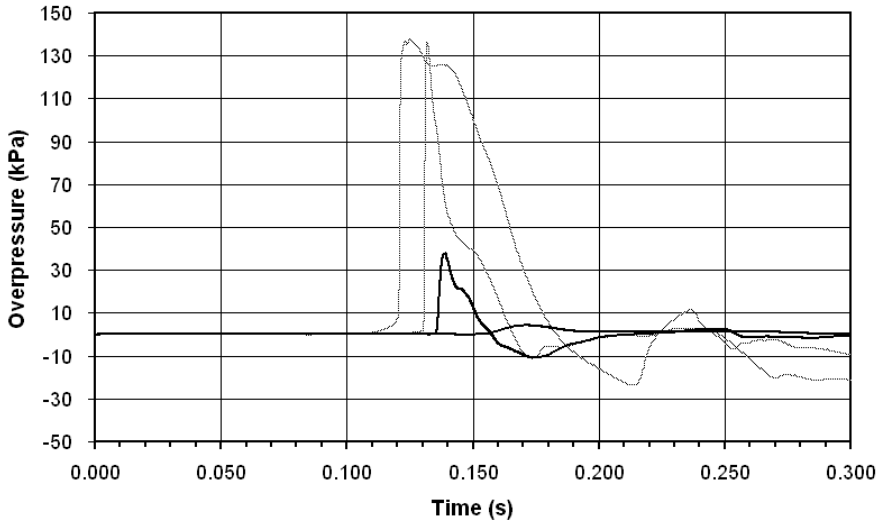

Figure 14. The simulated pressure dynamics: dotted (gray) lines – ceiling overpressure inside the tunnel at 34 m and 39 m from ignition source (inside the tunnel, 5.25 m and 0.25 m from the end of the tunnel respectively); solid lines – 40 m and 42 m from the ignition source (outside the tunnel, 0.75 m and 2.75 m respectively) at 1.2 m and 1.5 m from the ground level, respectively [1].

The LES model, calibrated previously to predict the dynamics of large-scale hydrogen-air deflagrations in the open atmosphere, is validated against experimental hydrogen-air explosions in a quite different environment of a 78.5 m long tunnel. The simulation reproduced the experimental results for both 20 vol. % and 30 vol. % hydrogen-air deflagrations, and included deflagrations in an unobstructed tunnel and in a tunnel with obstacles.

Hydrogen-air deflagrations in confined spaces present more severe hazards and associated risks compared to deflagrations in the open atmosphere. Indeed, overpressures registered during the near stoichiometric hydrogen-air deflagration of 1 kg of hydrogen in the tunnel are in the range 150-175 kPa [23]. This is essentially higher than overpressures of the order of only 6-10 kPa that were recorded during the stoichiometric hydrogen-air deflagration of significantly larger amounts of hydrogen of 55.5 kg in the open atmosphere [8]. Furthermore, once generated the pressure wave in the tunnel propagates without dissipation having the same overpressure along the whole tunnel. This again is different from deflagrations in open atmosphere where overpressure decayed proportionally to the inverse of distance.

The simulations confirmed the experimental observations that obstacles with a blockage ratio of 0.03, as per the tested configuration, have no significant effect on the maximum explosion pressure in the tunnel beyond the immediate vicinity of the obstacles. Both experiment and numerical simulations show small variance in maximum pressure along the tunnel. Based on the LES analysis it is demonstrated that side-on obstacle

overpressure can increase significantly due to reflection of the shock wave formed in the tunnel during the deflagration.

Vented deflagrations

Combustion of flammable mixture (i.e. deflagration) in a confined space (e.g. enclosure, room, warehouse etc.) will generate overpressure which may lead to damage and destruction to facilities and buildings. Provision of vents to release burned and unburned mixtures and to decrease overpressure is the most widely used and the most cost-effective strategy to mitigate deflagrations in confined spaces. If no venting is provided, the maximum pressures developed during the deflagration are typically 6 to 10 times the initial absolute pressure.

In this technique, weak areas (explosion vents) that fail early on in the explosion are deliberately incorporated into the item of equipment, venting the combustion products and reducing the explosion pressure generated inside the equipment. There are a number of methods used to seal the vents, such as thin membranes, bursting discs, lightweight covers held in place by magnetic fasteners and spring loaded doors. The opening pressure of the covers and the size of the vents are chosen to give explosion pressures below that which would damage the equipment. It may, however, be acceptable to allow some damage to the equipment, provided it does not result in damage to the adjacent area or injuries to nearby located personnel. It should also be ensured that the explosion is vented to safe areas so it causes no damage or injuries. The standards BS EN 14797:2006 “Explosion venting devices”, BS EN 14994:2007 “Gas explosion venting protective systems” [29] and NFPA 68“Standard on Explosion Protection by Deflagration Venting” [27] provide guidance on the design of explosion relief systems and the methods of available for vent sizing. However, even though venting is the most wide spread technique to mitigate explosions in an enclosure, there is no international reference standard related to the explosion venting protection system for particularly hydrogen application. European standard EN 14994 specifies the basic design requirements for the selection of a gas explosion venting protective system but it is not applicable to hydrogen explosion. NFPA 68 (USA) is the only national standard dealing with the inertial vent covers for hydrogen.

NFPA 68 recommends the following equation to calculate vent area for a targeted reduced overpressure:

$$F = \left\{\left[(0.127)\cdot\log_{10}(K_G)-(0.0567)\right]\cdot P_{red}^{-0.582}\right\}\cdot V^{2/3}+\left[(0.175)\cdot P_{red}^{-0.572}(P_{stat}-1)\right]\cdot V^{2/3}, \quad (3)$$

where F is the vent area, m^2; K_G is the deflagration index, bar·m/s; P_{red} is the reduced pressure, bar gauge; V is the volume of enclosure, m^3; P_{stat} is the static vent activation pressure, bar gauge. In general, the vent sizing formula (3) used in NFPA 68 (2007 edition) and its European version standard EN 14994 are not applicable to hydrogen. The “consensus” is to use a value of K_G for hydrogen equal to 550 bar·m/s.

Table 2 below gives examples of comparison between results obtained according to NFPA 68 (3) and an alternative vent sizing technique developed at Ulster University [28]. The Table gives experimental vessel volume, vent area and hydrogen vol. % in flammable composition. NFPA 68 (3) and Ulster University technique solved in two ways – for vent size targeting experimental overpressure, and for experimental overpressure keeping experimental vent size. Results of both solutions are presented in Table 3 along with deviation from experimental value expressed as percentage. Details of experiments and Ulster University vent sizing technique may be found in [28].

Table 2. A comparison between the experiments and predictions by the vent sizing technique [28] and the equation used in NFPA 68 standard [27].

Test	H_2, vol. %	V, m^3	F, m^2	Vent Area, F (m^2)					Reduced pressure, P_{red}					Use of NFPA[c]
				VST	%[a]	NFPA	%[a]	*Exp*[b]	*VST*[c]	%[a]	NFPA	%[a]	*Exp*[b]	
K10-15-C	10	6.85	0.0177	0.0780	342	0.362	1948	0.0177	3.67	126	260.00	15900	1.625	(+)
K10-15-R	10	6.85	0.0177	0.1070	506	0.448	2435	0.0177	3.67	224	260.00	22807	1.135	(+)
K10-15-N	10	6.85	0.0177	0.0890	405	0.391	2116	0.0177	3.67	158	260.00	18171	1.423	(+)
K10–25-C	10	6.85	0.0191	0.1188	142	0.514	947	0.0491	4.47	396	46.90	5111	0.900	(+)
K10-25-R	10	6.85	0.0191	0.1693	245	0.746	1420	0.0491	4.47	829	46.90	9657	0.481	(+)
K10-25-N	10	6.85	0.0191	0.1555	217	0.682	1291	0.0491	4.47	701	46.90	8305	0.558	(+)
K10-45-C	10	6.85	0.1590	0.2214	39	0.986	521	0.1590	0.54	79	6.49	2063	0.300	(+)
K10-45-R	10	6.85	0.1590	0.3500	120	1.584	897	0.1590	0.54	298	6.49	4707	0.135	(+)
K10-45-N	10	6.85	0.1590	0.4843	205	2.212	1292	0.1590	0.54	598	6.49	8340	0.077	(+)
K15-15-C	15	6.85	0.0177	0.0753	326	0.223	1163	0.0177	5.34	46	260.00	6985	3.670	(-)
K15-25-C	15	6.85	0.0191	0.1002	104	0.238	384	0.0491	4.20	27	46.90	1321	3.300	(-)
K15-45-C	15	6.85	0.1590	0.2378	50	0.311	95	0.1590	2.68	27	6.49	209	2.100	(-)
K15-45-R	15	6.85	0.1590	0.4534	185	0.454	185	0.1590	2.68	141	6.49	485	1.110	(+)
K15-45-N	15	6.85	0.1590	0.4139	160	0.422	165	0.1590	2.68	113	6.49	417	1.255	(+)
K20-15-C	20	6.85	0.0177	0.0536	203	0.185	947	0.0177	6.14	22	260.00	5069	5.030	(-)
K20-25-C	20	6.85	0.0191	0.0819	67	0.196	300	0.0491	5.13	13	46.90	931	4.550	(-)
K20-45-C	20	6.85	0.1590	0.1643	3	0.222	40	0.1590	3.74	1	6.49	75	3.700	(-)
P1-C	29.6	0.95	0.20	0.2132	7	0.110	-45	0.2000	1.35	8	0.45	-64	1.250	(+)
P2-C	29.6	0.95	0.30	0.4176	39	0.233	-22	0.3000	0.74	85	0.26	-35	0.400	(+)
SRI-30F	30	37.4	7.48	11.95	60	1.112	-85	7.48	1.72	33	0.05	-96	1.300	(-)
SRI-20F	20	37.4	7.48	11.82	58	2.434	-67	7.48	0.78	122	0.05	-85	0.280	(-)
SRI-15F	15	37.4	7.48	7.48	0	3.127	-58	7.48	0.23	0	0.05	-77	0.220	(-)

Notes: In column "Test": C – central ignition, R – rear to vent ignition, N – near vent ignition, F – floor ignition. *VST* stands for vent sizing technique.

[a] - deviation of prediction from corresponding experimental value, calculated by formula: $100\times(A_{pred} - A_{exp})/A_{exp}$, where A is reduced pressure or vent area.

[b] - experimental data.

[c] - applicability of NFPA 68 (2007) to predict particular experiment: sign (+) in the last column means that the equation (3) is applicable, sign (-) refers to experimental conditions outside the specified range of applicability of the equation (3).

The Ulster University vent sizing correlations were applied to tunnel explosions as follows: the volume of uniform hydrogen-air mixture represents an "enclosure volume" and the "enclosure vent area" is equal to double the cross sectional area of the tunnel. More details on comparison between experimental data and predictions by the vent sizing technology and the equation (3) with K_G=550 bar·m/sec are given in [28].

From Table 2 it can be seen that the NFPA 68 [27], and hence EN14994 [29], significantly overestimates vent areas and reduced pressure (sometimes up to 6985%) in some cases and underestimate in other cases, thereby being not conservative, by comparison to the vent sizing correlations which are demonstrated to be essentially closer to experiment predictions.

The procedure for calculating the vent area for an empty enclosure fully filled with a quiescent hydrogen-air or enclosure with insignificant influence of obstacles is as follows:

1. Calculate the dimensionless reduced explosion overpressure $\pi_{red} = P_{red}/P_i$
2. Determine the dimensionless static activation pressure $\pi_v = (P_{stat} + P_i)/P_i$

3. Calculate the dimensionless pressure complex using data from step 1 and 2 $\pi_{red}/\pi_v^{2.5}$

4. Calculate the value of the turbulent Bradley number Br_t by the use of one of the following two equations depending on the value of the above mentioned dimensionless pressure complex $\pi_{red}/\pi_v^{2.5}$:

If $\pi_{red}/\pi_v^{2.5} \leq 1$, then use equation: $\frac{\pi_{red}}{\pi_v^{2.5}} = 5.65 \cdot Br_t^{-2.5}$ (4)

If $\pi_{red}/\pi_v^{2.5} \geq 1$, then use equation: $\frac{\pi_{red}}{\pi_v^{2.5}} = 7.9 - 5.8 \cdot Br_t^{-2.5}$ (5)

5. Using Figure 15 below, determine the appropriate values of the laminar burning velocity and the expansion ratio for the suitable hydrogen-air mixture (by volumetric fraction of hydrogen in air). For instance, for stoichiometric hydrogen-air mixture at NTP, the following values can be used for the purpose of vent sizing: E_i=6.88, S_{u0}=1.96 m/s [30,31]. The influence of the initial temperature on the laminar burning velocity can be extrapolated from the formula (6):

$$S_{ui} = S_{u0} \cdot \left(\frac{T}{298}\right)^{m0} \quad (6)$$

where S_{u0} is the laminar burning velocity at 298 K (Figure 15), T is the initial temperature, m_0 is the temperature index that can be taken as m_0 = 1.7 for near stoichiometric hydrogen-air mixtures [32]; and S_{u0} is the laminar burning velocity at 298 K and T_i is the initial temperature in the enclosure.

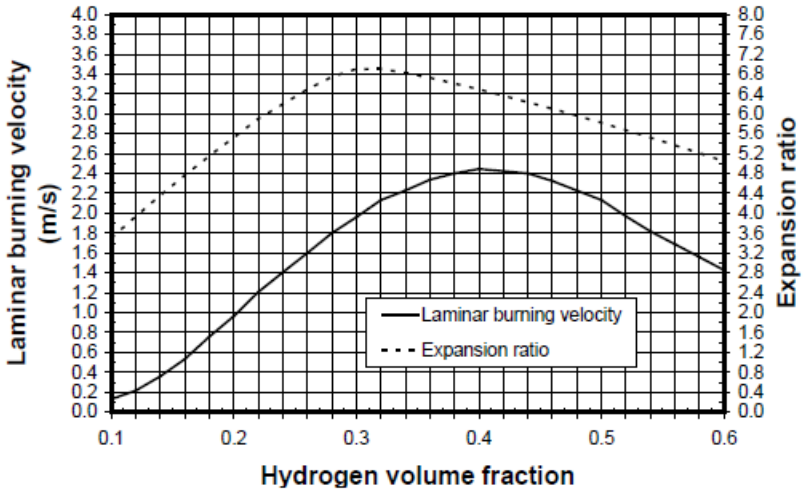

Figure 15. Laminar burning velocity and expansion ratio for hydrogen-air mixtures at initial pressure 1 bar and temperature 298 K.

6. Determine the vent area by numerical solving of the following equation:

$$\frac{Br_t \cdot \sqrt[3]{36\pi_0} \cdot V^{2/3}}{c_{ui} \cdot \sqrt{E_i / \gamma_u}} = \frac{A(1+\pi_v)^{0.4} \cdot \left[1 + 0.5 \cdot \left(\frac{A}{V^{2/3}} \cdot \frac{c_{ui}}{S_{ui}(E_i - 1)}\right)^{0.8}\right]^{-0.4}}{(1 + e \cdot V^g)^{0.4} \cdot S_{ui} \cdot (E_i - 1)} \quad (7)$$

where empirical coefficients e=2 and g=0.94, and other parameters are:

A is the vent area of an explosion venting device, in m^2;

Br_t is the turbulent Bradley number;

c_{ui} is the speed of sound at initial conditions (m/s); $c_{ui} = (\gamma_u R T_{ui}/M_{ui})^{0.5}$

E_i is the expansion ratio of combustion products, $E_i = M_{ui}T_{bi}/M_{bi}T_{ui}$

M is the molecular mass, in kg/mol

p_i is the initial absolute pressure, in bar abs
p_{red} is the reduced overpressure, in bar gauge
p_{stat} is the static activation pressure, in bar gauge
R is the universal gas constant, R = 8.31 J/K/mol
S_{ui} is the burning velocity at initial conditions, in m/s
V is the enclosure volume, in m^3
γ_u is the specific heats ratio for unburned mixture
π_{red} is the dimensionless maximum explosion overpressure (reduced pressure)
$\pi_{red} = p_{red}/p_i$
π_v is the dimensionless static activation pressure, $\pi_v = (p_{stat} + p_i)/p_i$
$\pi_0 = 3.14$.

The correlations have been calibrated against experimental data for hydrogen-air deflagrations for the following range of conditions:

$L/D \leq 5.43$;
$V \leq 37.4$ m^3;
$0.005 < A/V^{2/3} < 0.34$;
0 kPa $\leq p_{stat} \leq$ 13.5 kPa;
p_i =1 bar abs.
$0.3 \leq \pi_{red} \leq 5$.

The method of vent sizing presented above allows the estimation of the effect of initial pressure and temperature of the explosive gaseous atmosphere in the protected enclosure. In 90% of the cases, this methodology has been shown to give closer predictions than NFPA 68 standard [27].

The prediction capability of vent sizing methodology is demonstrated on the experimental data for hydrogen-air deflagrations ("P" series in Table 2). Pasman et al. (1974) carried out the experiments in a 0.95 m^3 cylindrical vessel of 0.97 m diameter and 1.50 m length [33]. A flange was located at the back of the vessel to accommodate a rupture membrane. The hydrogen-air mixture was ignited in the centre of the vessel. The experiments with a stoichiometric (29.6 vol. %) hydrogen-air mixture were performed with two different vent areas of 0.3 m^2 (0.62 m diameter) and 0.2 m^2 (0.50 m diameter). The initial pressure in the vessel was equal to 101.8 kPa and the temperature was 281 K. Experimental pressure dynamics is given in Figure 16 in comparison with numerical simulation results.

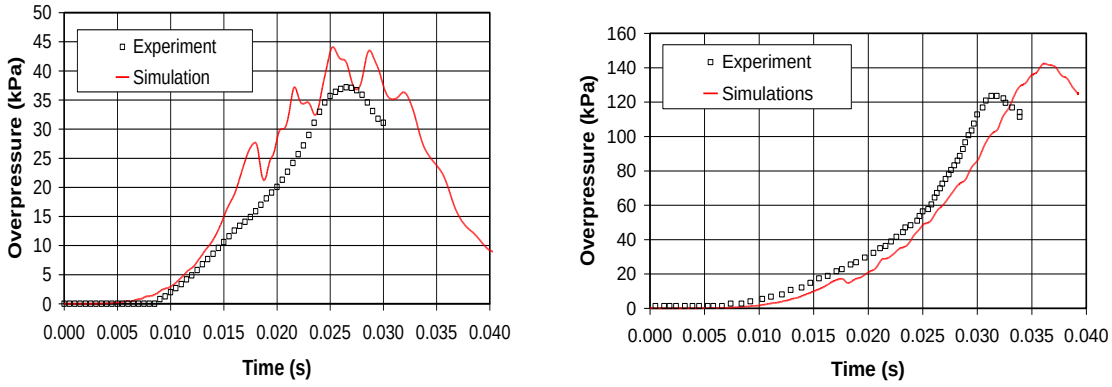

(a) (b)

Figure 16. A comparison of experimental and simulated overpressure values for deflagrations vented through the vent with: (a) 0.62 m in diameter, (b) 0.50 m in diameter.

Calculation means for overpressure assessment and vents sizing will be discussed in the lecture 'Safety of hydrogen use indoors'.

Localised hydrogen-air deflagrations

Ignition of flammable hydrogen-air mixture at central part of enclosure or at a rear wall typically leads to a higher maximum deflagration overpressure compared to a near-vent ignition. Delayed ignition of hydrogen jets and releases forming localised highly turbulent hydrogen-air cloud may lead to significant overpressure in ignition vicinity even though average concentration in a vessel may be low (e.g. ~1 vol. %). Vented deflagration of a stratified hydrogen-air mixture may lead to significantly higher overpressure compared to the lean uniform hydrogen-air composition with the same hydrogen inventory (i.e. stored hydrogen mass). Congestion (i.e. high blockage ratio) inside the enclosure accelerates flame and causes higher deflagration overpressures. The deflagration overpressure decreases when the vent surfaces are increased. The larger the vent area, the higher the concentration of the flammable mixture can be without destroying the enclosure. The effectiveness of deflagration venting is not affected by the vent orientation (either horizontal or vertical). A single vent of larger area or multiple vents will suppress flame acceleration and higher deflagration overpressures.

Computational Fluid Dynamics (CFD) can be used for complex geometries, multiple vents and parameters which cannot be described by classical analytical engineering tools. CFD models are capable to reproduce major experimentally observed deflagration dynamics features. Care should be taken to ensure that CFD models are validated for the same range of parameters for which they are applied: hydrogen concentrations, enclosure scales, congestion, vent size, etc.

Closed vessel deflagration

A limitation of hydrogen inventory is one of safety strategies for indoor use of hydrogen. A thermodynamic model may be used to predict maximum mass of hydrogen, which is allowed to be released in an enclosure without causing destructive overpressure in case of its combustion. The model presumes that localised hydrogen-air mixture fills the enclosure only partially and burns in a completely sealed enclosure.

The upper limit of hydrogen inventory may be defined using 10 kPa overpressure as a criterion for minor damage (like windows breakage, etc.). A model to find the hydrogen inventory limit for use in poorly ventilated enclosures or enclosures without specially provided ventilation was developed and validated in HyIndoor project (see D5.1 "Guidelines on fuel cell indoor installation and use", www.hyindoor.eu) [34]. This issue will be considered in the following Lecture 'Safety of hydrogen use indoors'.

The lowest hydrogen inventory, which provided 10 kPa overpressure, was obtained for hydrogen volumetric (vol.) fraction in the mixture φ=0.04 (i.e. LFL) and vol. fraction of mixture in enclosure Φ=0.0786, giving total H_2 vol. fraction in a sealed enclosure $\Phi \cdot \varphi = 3.14 \cdot 10^{-3}$**,** which is smaller than typically considered as a safety threshold LFL of 0.04! This volumetric fraction corresponds to *0.261 g of hydrogen per 1 m^3 of enclosure volume.* Note that local damage may still occur to the structure if a layer of higher hydrogen concentration forms within the room/enclosure and detonation occurs, such as in areas of high congestion [35].

Vented deflagration

When inventory is larger than the specified limit 0.261 g H_2/m^3, the use of other mitigation techniques should be considered (natural/forced ventilation to exclude flammable mixture formation, deflagration venting, etc.). It is expected that venting of partial-volume or stratified mixture deflagrations should be easier than that of full-volume explosions due to lower amount of hydrogen. For the same amount of hydrogen, deflagrations of non-uniform layered mixtures can generate overpressure above that for uniform mixture deflagration. The maximum overpressure depends strongly on the portion of mixture with the largest burning velocity (i.e. largest hydrogen concentration in case of lean mixtures). Method to calculate vent area to avoid

destructive overpressure in case of localized mixture deflagration was described and validated within HyIndoor project too [34]. This method will be considered in the following lecture.

Detonations

For vented deflagrations the overpressure may be anywhere between overpressures in open atmosphere deflagration and closed vessel deflagration. In a closed vessel deflagration, the maximum pressure to initial pressure ratio is essentially higher and for stoichiometric mixture at NTP it equals to 8.15 [36]. *Detonation* is the worst case of accidental hydrogen combustion: characteristic overpressure in stoichiometric hydrogen-air mixture detonation front is even higher than for closed vessel deflagration - 1.56 MPa, and it propagates faster than the speed of sound - at 1,968 m/s [36]. The detonation wave is a complex of precursor shock and combustion wave and its description can be found elsewhere [37]. Detonation front thickness is a distance from the precursor shock to the end of reaction zone where the Chapman-Jouguet condition (sonic plane) condition is reached and it is typically of the order 0.1 cm.

Deflagration-to-detonation transition

Hydrogen is prone to the deflagration-to-detonation transition (DDT). DDT can happen in different environment, including tubes, enclosures, etc. Different mechanism are responsible for a flame front acceleration to a velocity close to the speed of sound in an unburned mixture, including but not limited to turbulence in an unburned mixture, turbulence generated by flame front itself, and various instabilities [1]. Then, there is a jump from the sonic flame propagation velocity to the detonation velocity, which is about twice of the speed of sound at least for near stoichiometric hydrogen-air mixture [1]. The DDT phenomenon is still one of the challenging subjects for combustion research.

The experimentally observed run-up distance (distance from the ignition point to the location of DDT) in stoichiometric hydrogen-air mixture in a tube has typical length to diameter ratio of 15-40. The presence of obstacles in a tube can significantly reduce the run-up distance for DDT. The initiation of detonation during DDT is thought to happen in a so-called ‘hot spots’, which potentially could be located within the turbulent flame brush or ahead of it, e.g. in a focus of a strong shock reflection. The peculiarities of DDT mechanisms are not affecting parameters of a steady-state detonation wave following it [1].

Safety measures to exclude the potential DDT are very important. Indeed, while the deflagration of quiescent stoichiometric hydrogen-air cloud in the open atmosphere generates pressure wave of only 0.01 MPa (below a level of eardrum injury), the detonation of the same mixture would be accompanied by a blast of more than two orders of magnitude higher pressure of about 1.5 MPa (far above the fatal pressure of about 0.08-0.10 MPa) [1].

DDT was observed during mitigation of deflagration in an enclosure by the venting technique. Venting of a 30 vol. % hydrogen-air deflagration in a room-like enclosure with an internal jet camera and initially closed venting panels resulted in the DDT with overpressures up to 3.5 MPa in experiments performed by Dorofeev et al. in the Kurchatov Institute (Russia) [38]. The DDT was initiated a few milliseconds after the destruction of the venting panels. The formation of an outflow followed by a localized explosion inside the enclosure near the panel was confirmed. No effect of the igniting jet size, emerging from the camera jet, on the onset of detonation was observed. The volume size of the jet camera also had no effect, indicating the local character of the detonation onset. Authors [38] suggested that the onset of detonation was not directly connected with jet ignition, but was specifically linked to the sudden venting. Indeed, a needle-like structured flame front with developed combustion surface can be induced by the venting as observed in experiments of Tsuruda and Hirano [39]. Flame front instabilities, in particular Rayleigh-Taylor instability, and rarefaction waves propagating into the enclosure after the destruction of the venting panel increase the mixing of the unburnt mixture and combustion products that can facilitate formation of ‘hot spots’. In partially reacted

mixtures this may create an induction time gradient thereby establishing the conditions for the DDT. The possibility of the DDT initiation during a reflection of a pressure wave generated by the camera jet combustion cannot be excluded as well (this could “naturally” coincide with the start of the venting panel opening) [1].

The DDT was observed in the large-scale test carried out by Pfortner and Schneider (1984) in Fraunhofer ICT (Germany) [40]. The experimental set up included a “lane” (two parallel walls 3 m apart with height 3 m and length 12 m) and an enclosure (driver section) of sizes LxWxH=3.0x1.5x1.5 m (6.75 m^3 volume) with an initially open to the “lane” vent of 0.82x0.82 m. The “lane” and the enclosure were filled with the same 22.5 vol. % hydrogen-air mixture kept under a plastic film. Venting of 22.5 vol. % hydrogen-air deflagration initiated at the rear wall of the enclosure by five ignitors into the partially confined space simulating a “lane” resulted in the DDT. At a time of 54.61 ms after ignition the DDT occurred in the “lane” at the ground level, when the accelerated flame emerged from the driver section touched the ground [40].

The run-up distance to DDT

The distance from the ignition point to the location of DDT, i.e. run-up distance X_D, decreases with increase of pressure (Figure 17). For a pipe of diameter 105 mm at the initial pressure of 1 bar it is about 70 cm and at pressure of 5 bar it is about 7 cm (correlation for X_D is applicable to tubes with internal diameter more than 20 detonation cell sizes, $d > 20\lambda$; to be discussed below) [41].

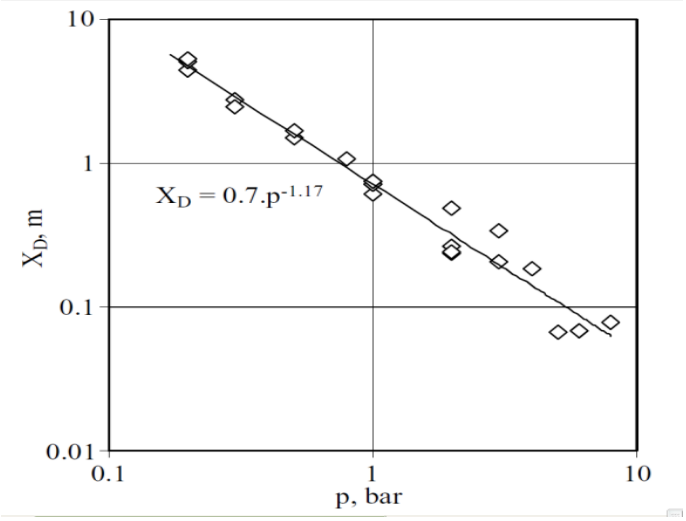

Figure 17. The run-up distance to the DDT as a function of the initial pressure [41]

Detonability limits and factors affecting the detonability range

The upper and lower detonation limits (UDL and LDL) are the maximum and minimum concentrations of hydrogen in air or oxygen for stable detonations to occur. These limits are controlled by the size and geometry of the environment as well as the concentration of the fuel [42]. They are different from flammability limits, which determine limits for slow flame propagation rather than limits for propagation of supersonic detonation wave. Detonability limits are always within the flammability range. The detonability limits are not fundamental characteristics of the mixture as they strongly depend on the nature and size of an experimental set-up. Indeed, a diameter of the tube, where detonation can propagate, should be of the order of a detonation cell size λ (see below).

The detonability range mentioned in technical report ISO/TR 15916:2004 [43] is 18-59 vol. % of hydrogen in air. The detonation range of 13-70 vol. % is reported for hydrogen-air in a 43 cm diameter tube [44]. Even lower value of detonability limit of 12.5 vol. % was observed in the Russian detonation test facility RUT, the

largest of its kind [1]. The widest detonability range of hydrogen in air 11-59 vol. % is recommended by Alcock et al. (2001) [6].

Detonability range depends on the nature of the oxidizer. For example, the detonability range for hydrogen-air mixtures is reported as 18.2-58.9 vol. % interval, while for hydrogen-oxygen mixtures it is 15-90 vol. % [45].

An increase in temperature (T) from 293 to 373 K leads to a widening of detonability range: the LDL is reduced from 11.6 to 9.4 vol. %, whilst the UDL is increased from 74 to 76.9 vol. % for hydrogen-air mixtures.

The detonability range strongly depends on the addition of diluents to hydrogen-containing mixtures. The effects of three diluents, carbon dioxide (CO_2), water (H_2O) and nitrogen (N_2), on both detonability and flammability limits are shown in Figures 18-20.

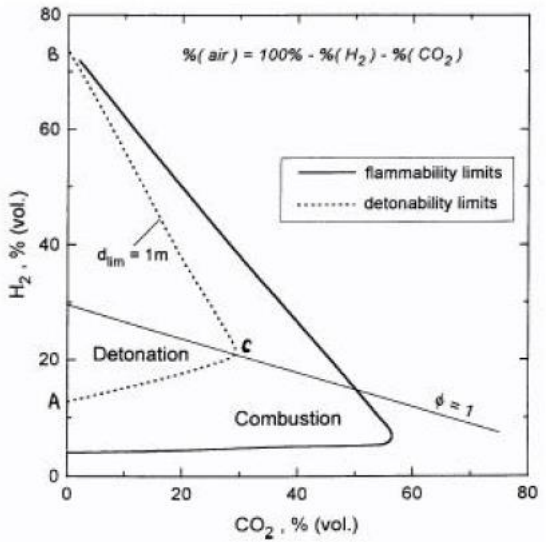

Figure 18. Effect of carbon dioxide addition to hydrogen-air mixtures on the detonability/flammability range [46].

Carbon dioxide ($CO_{2)}$ significantly changes the detonability range of hydrogen-air mixture: it is marginally reduced in the presence of this diluent (Figure 18).

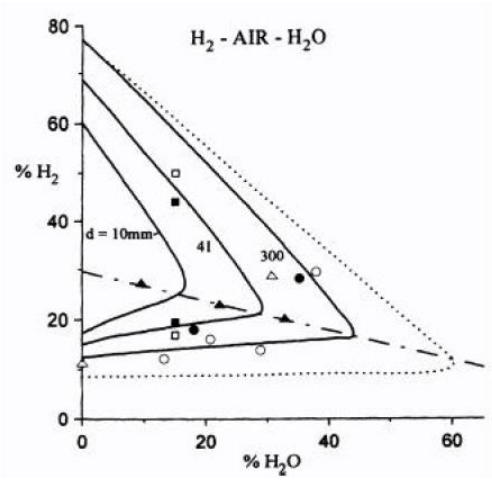

Figure 19. Effect of water addition to hydrogen-air mixtures on the detonability range [46].

Detonability range is also significantly reduced in the presence of water. A size of a pipe diameter also affects the detonability range of hydrogen-air mixtures (Figure 19).

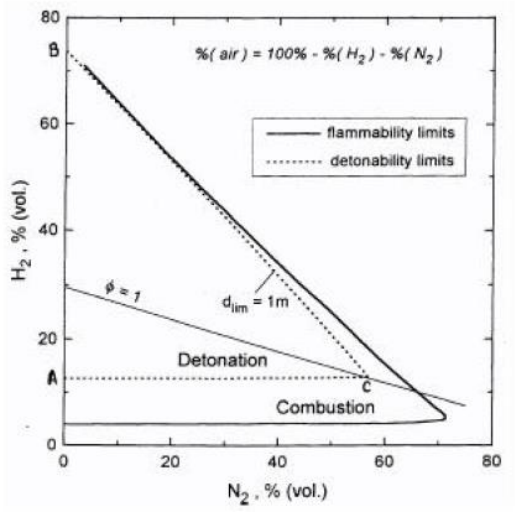

Figure 20. Effect of nitrogen addition to hydrogen-air mixtures on the detonability range [46].

In the presence of nitrogen (N_2) the UDL is greatly reduced as the concentration of diluent increases. Both LFL and LDL remain almost unchanged.

Detonation cell size and structure of the detonation front

Once initiated, detonation will propagate as long as the mixture is within the detonability limits subject to a sufficient size of the cloud. A detonation wave has a complex 3D structure with a characteristic fish-scale pattern as shown in Figures 21 and 22 [47], and then in Figure 24 [51].

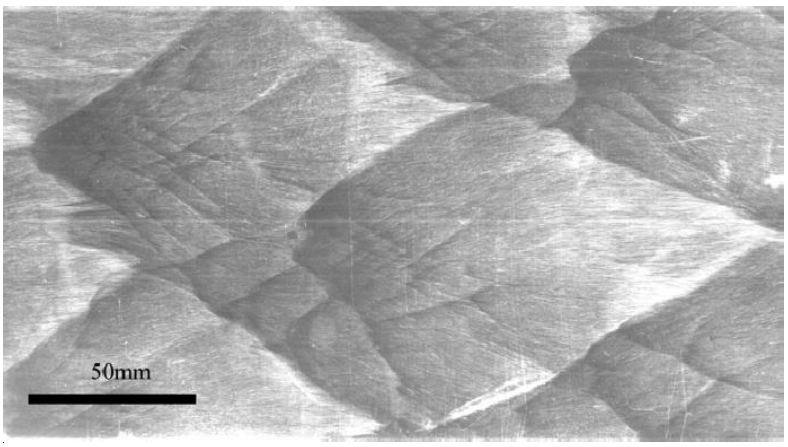

Figure 21. A cellular structure of the detonation wave (detonation propagated from left to right) [47].

Detonation can propagate through channels with a characteristic size of the order of a *detonation cell size* (λ). The detonation cell size is a measure of reactivity of a fuel-oxidizer mixture. The wave front is not planar and composed of reaction cells. Highly reactive mixtures such as acetylene-air have very small cell sizes (about 1 mm).

Detonation cell lengths for stoichiometric hydrogen-air and hydrogen-oxygen at initial pressures of 101.3 kPa are reported to be 15.9 mm and 0.6 mm, respectively in [48]. This means that hydrogen-oxygen detonation can propagate through smaller size channels compared to hydrogen-air detonation. The detonation cell size is a function of a mixture composition. Dependence of detonation cell size (λ) for hydrogen-air mixtures on hydrogen concentration is given in Figure 23 [49]. In another experimental paper the values of detonation cell size for a stoichiometric hydrogen-air mixture were measured as 1.1-2.1 cm [50].

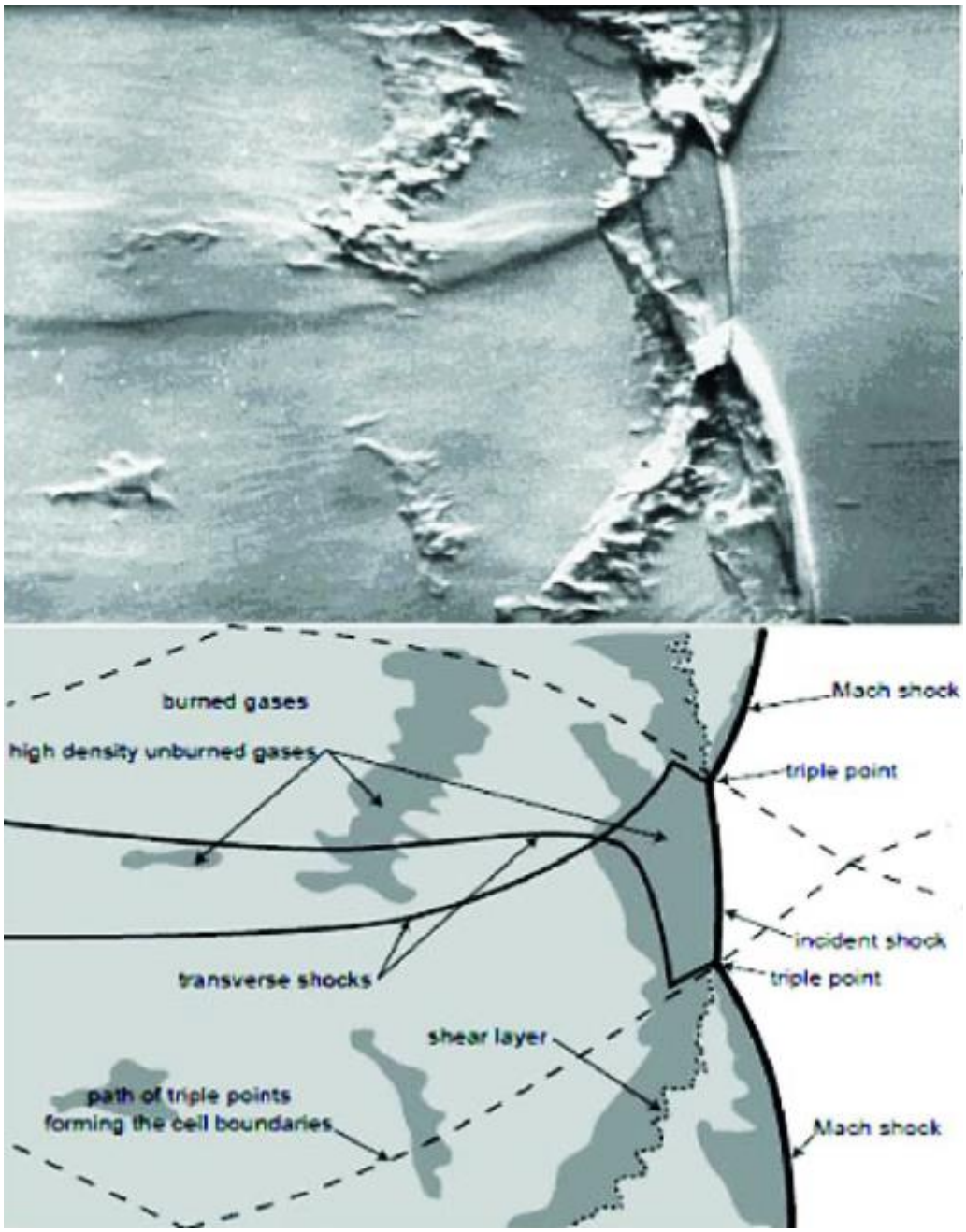

Figure 22. A schlieren photograph of the hydrodynamic detonation structure and explanatory sketch [47].

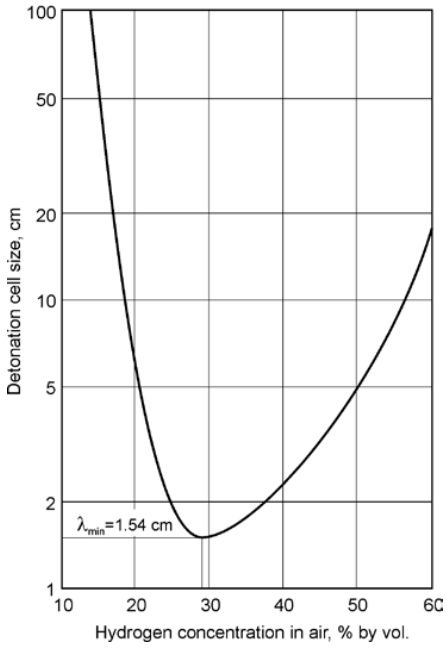

Figure 23. Detonation cell size as a function of hydrogen concentration in air [49].

A detonation cell size increases as it approaches the detonability limits. Thus, the larger is the scale of an experimental apparatus the smaller is the value of LDL (the larger is the UDL). The detonability limits of hydrogen-air mixture of the same concentration expand with the scale of a flammable cloud. This explains the difference between the lower detonability limit of hydrogen 11 vol. % reported by Alcock et al. (2001) [6] and the underestimated value of 18 vol. % suggested by the international standard ISO/TR 15916:2004 [43].

A structure of a detonation front is shown schematically in Figure 24. A 2D illustration of the detonation front structure is given below according to Zeldovich, von Neumann and Doring (ZND) models.

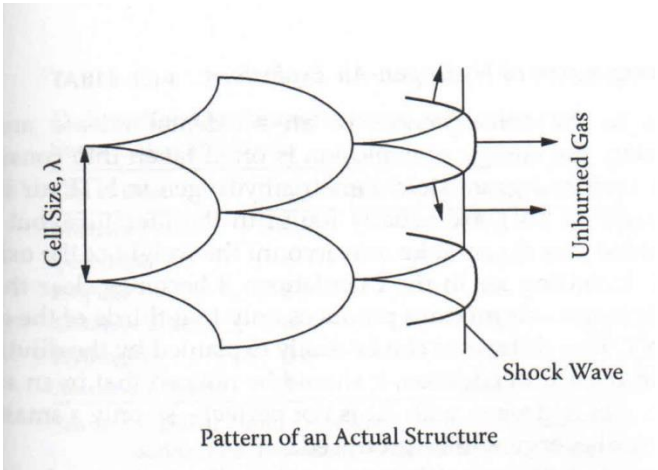

Figure 24. A 2D representation of a detonation front structure [51].

The cell size decreases with the pressure increase for hydrogen-air mixtures. The cell width of hydrogen-air detonations increases significantly with the concentration of diluents (e.g. carbon dioxide or water).

Critical tube diameter for detonation onset

Detonation may only occur if the size of a duct or mixture volume is sufficiently higher compared to the detonation cell size λ (if supersonic flow regime is developed).

- $D > \lambda / \pi$, where D is a smooth tube internal diameter;
- $d > \lambda$, where d is the transverse dimension of the unobstructed passage in a channel with obstacles;

- $L>7\lambda$, where L is a more general characteristic size defined for rooms or channels;
- $D_{jet}>(14\text{-}24)\lambda$, where D_{jet} refers to the jet exit diameter.

For the congested area with stoichiometric hydrogen-air mixture DDT observed in a cloud containing 4 g of hydrogen.

Direct initiation of detonations

The ability of a hydrogen-air mixture to direct initiation of detonation is greater than that of hydrocarbons. The direct initiation of hydrogen-air mixture detonation is possible by 1.1 g of high explosive tetryl [36]. Only 1.86 g of high explosive TNT (trinitrotoluene) is needed to initiate detonation in 34.7 vol. % hydrogen-air mixture in the open atmosphere. However, for 20 vol. % hydrogen-air mixture the critical TNT charge increases significantly to 190 g [36]. For comparison, release of energy during explosive reaction of 1 g TNT is arbitrarily standardized as 4.184 kJ (a gram of TNT releases 4.1–4.602 kJ upon explosion, see Wikipedia), and the lower heat of combustion of 1 g of hydrogen is equal to (241.7 kJ/mol / 2.016 g/mol) = 119.89 kJ. Thus, the TNT equivalent of hydrogen is high: 28.65, i.e. 28.65 g of TNT is energetic equivalent of 1 g of hydrogen [1, 36].

The ignition energy requirements for hydrogen are among the lowest of any combustible fuel-oxygen mixture (MIE of GH_2 in air at NTP is 0.017 mJ). For many hydrogen-oxygen compositions with no dilution, initiation by a spark (for example, 1-5 mJ in experiments [52]) or flame source can produce a full detonation. In comparison, hydrogen-air mixture detonation requires essentially stronger initiation by at least a 1-2 g explosive charge (see Figure 25).

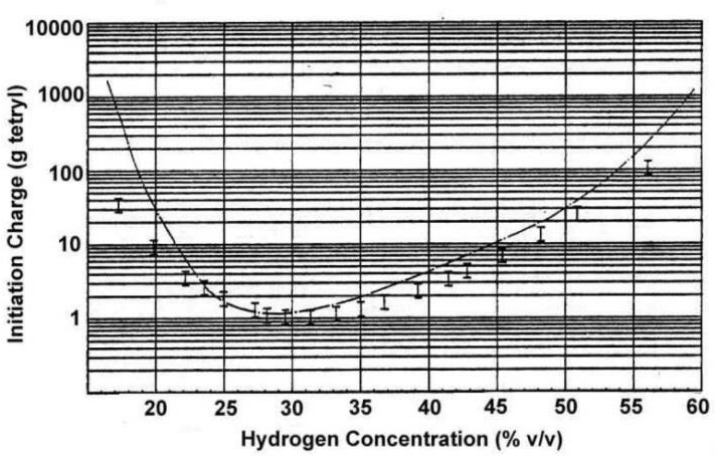

Figure 25. Minimum initiation energies for direct detonation of hydrogen-air mixtures [53].

The minimum initiation energies for deflagrations and detonations of different fuels are indicated in Table 3. The minimum energy required to initiate a detonation of hydrogen air-mixture is around $1\cdot10^7$ mJ, which is about nine orders of magnitude higher than MIE for deflagration (0.017 mJ).

Table 3. The minimum values of energy needed for the initiation of deflagration and detonations of hydrogen, methane and propane.

Type of fuel	Minimum Ignitions/Initiation Energy	
	Deflagration, mJ	*Detonation, mJ*
Hydrogen	0.017	$1.0 \cdot 10^7$
Methane	0.25	$2.3\cdot 10^{11}$
Propane	0.28	$2.5 \cdot 10^9$

Dimensionless detonation pressure (P_1/P_0, equilibrium Chapman-Jouguet values) and temperature (T_1/T_0) for hydrogen-air and hydrogen-oxygen mixtures are given in the Table 4 below. The P_1/P_0 and T_1/T_0 ratios give the pressure and temperature rise across the detonation shock.

Table 4. Detonation parameters of stoichiometric hydrogen-air and hydrogen-oxygen mixtures as a function of hydrogen concentration [42]

H_2 concentration, % v/v	T_0, K	P_0, kPa	T_1/T_0	P_1/P_0	T_0, K	P_0, kPa	T_1/T_0	P_1/P_0
Hydrogen-air mixture								
18.3	298	101.3	7.657	12.154	298	10.1	7.580	12.111
25	298	101.3	9.257	14.605	298	10.1	8.870	14.223
50	298	101.3	8.706	13.713	298	10.1	8.482	13.555
59	298	101.3	7.678	12.144	298	10.1	7.601	12.119
Hydrogen-oxygen mixture								
5	298	101.3	3.118	4.880	298	10.1	3.119	4.882
25	298	101.3	9.034	14.289	298	10.1	8.660	13.896
50	298	101.3	11.646	17.857	298	10.1	10.537	16.616
75	298	101.3	12.111	18.671	298	10.1	10.834	17.250
90	298	101.3	8.576	13.584	298	10.1	8.327	13.393

Detonation of 30% hydrogen-air mixture

The LES model was applied to simulate a hemispherical detonation of 30 vol. % hydrogen-air mixture in a polyethylene balloon with the radius of 5.23 m propagating through unobstructed environment [23]. Direct initiation of the detonation was at the ground level. Figure 26 provides snapshots of the experiment. Blast wave overpressure dynamics was recorded at distance 15.6 m and the corresponding blast wave impulse was calculated.

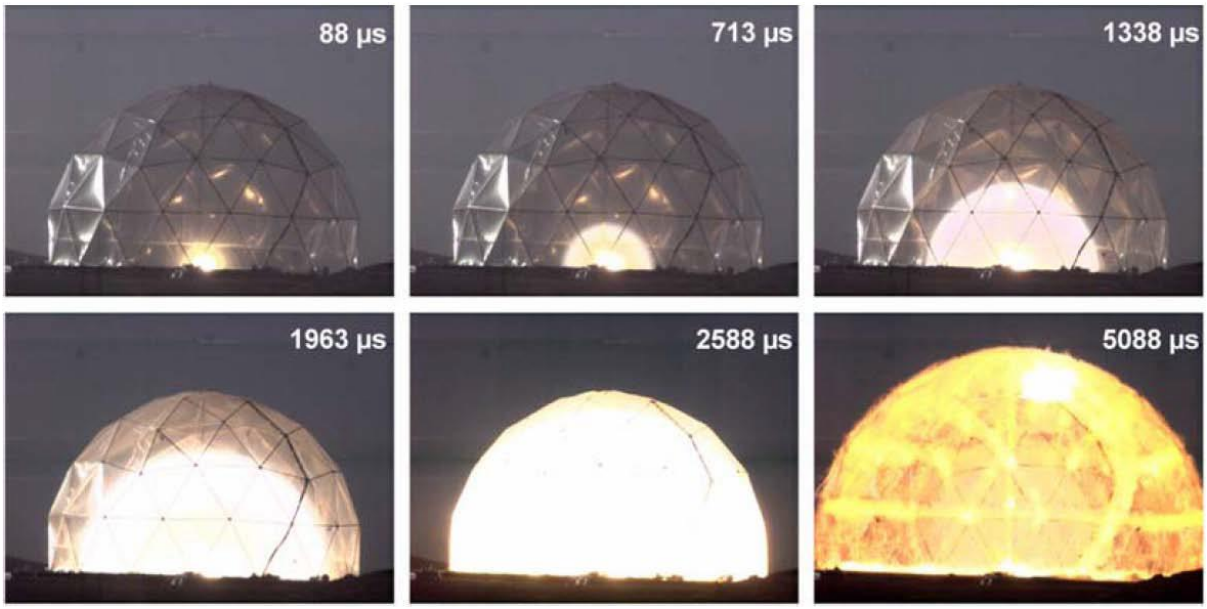

Figure 26. Hemispherical detonations of hydrogen-air mixture (30 vol. %) in a polyethylene balloon (radius 5.23 m) [23].

The detonation (Chapmen-Jouguet) velocity for 30 vol. % hydrogen-air mixture determined according to [54] was *D*=1,977 m/s [1], Chapman-Jouguet pressure 15.3 MPa [1]. Experimental dynamics of a blast wave from detonation at distance 15.61 m from the ignition point is shown in Figure 27 overlapped by simulation results. The agreement is in general acceptable, with 25% under prediction of the simulated blast overpressure in the peak.

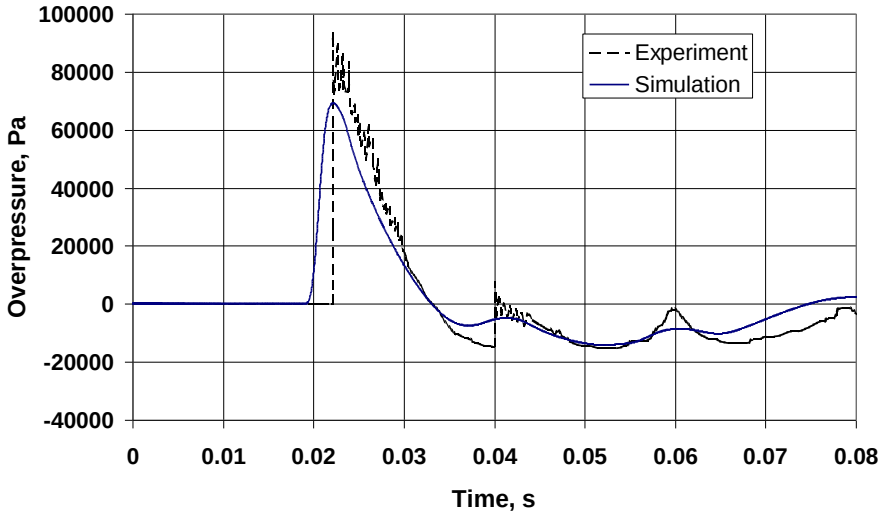

Figure 27. The experimental and simulated blast wave overpressure dynamics at a distance of 15.61 m [1].

Contrary to the blast wave pressure dynamics, the calculated impulse is in good agreement with experiment (Figure 28). This is thought due to correct energy balance provided by the model.

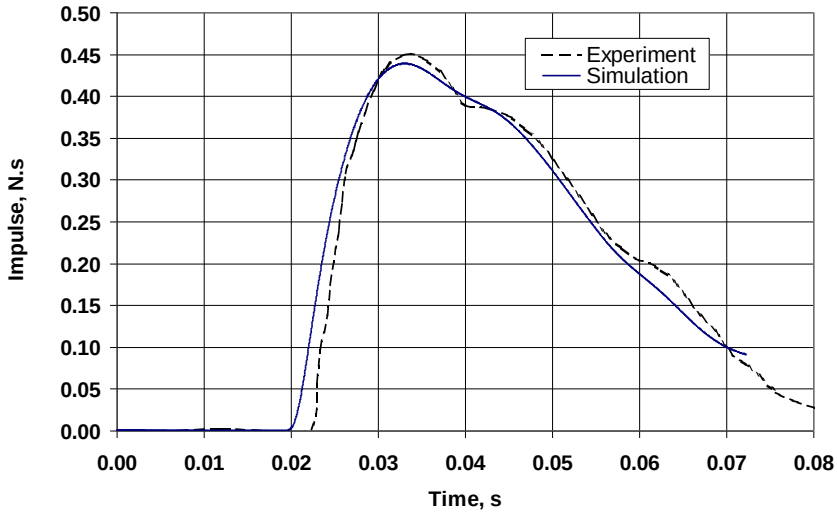

Figure 28. The experimental and simulated blast wave impulse at distance 15.61 m [1].

The effects of blast waves on people and buildings

The blast waves are harmful in a number of ways. These can be classified as primary, secondary and tertiary effects [55].

- Primary effects:
  - Damage to hearing
  - Damage to lungs and other internal organs
- Secondary effects:
  - Injuries due to flying debris (e.g. glass shards)
  - Collapse of structures on to people resulting in severe injuries or death
- Tertiary effects:
  - A whole-body displacement of an individual

It is not only overpressure that causes harm but also impulse imparted on a person or object, where person is located and what personal equipment he/she wears.

The methodology developed at Ulster [56] allows the users to determine hazard distances, for humans and buildings, in case of a high-pressure hydrogen tank (either stand-alone or on-board of FC vehicle) rupture in a fire. The methodology proposes a set of nomograms for graphical determination of hazard distances from stand-alone (Figure 29a and Figure 30a) and under-vehicle (Figure 29b and Figure 30b) tank rupture in a fire.

The temporary loss of hearing described by Baker et al. [57] that occurs at overpressure above 1.35 kPa and impulses above 1 Pa·s is considered as a threshold for "No harm" to humans. The thresholds for "injury" and "fatality" for humans and the thresholds for buildings represented in Tables 5 and 6, were adopted from [58].

Table 5. The thresholds of overpressures for harm to humans (outdoors).

Effect	**Overpressure, kPa**
Temporary threshold shift [57]: "no harm" threshold for hazard distance (evacuation perimeter)	1.35
1% probability of eardrum rupture (chosen as "injury" threshold) [58]	16.5
1% probability of fatality-lung haemorrhage (chosen as "fatality" threshold) [58]	100

Table 6. The thresholds of overpressure for buildings damage [58].

Damage	**Overpressure, kPa**
Minor damage of the house	4.8
Partial demolition of the house-remains inhabitable	6.9
Almost total destruction of the house	34.5-48.3

The harm criteria for humans and damage criteria for buildings described above in the Tables 5 and 6 are used in the nomograms below for the determination of the hazard distances from a rupture of stand-alone and under-vehicle high-pressure hydrogen tanks of different volume with different pressure.

Rupture of a stand-alone tank in a fire

Figure 29a allows hazmat officers to evaluate hazard distances to humans from a stand-alone tank rupture in a fire, whilst Figure 29b - to buildings from a stand-alone tank.

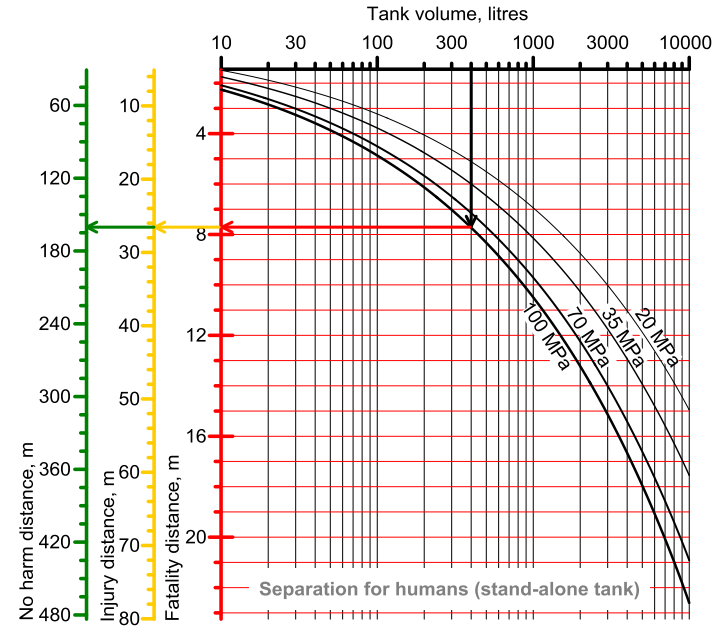

(a)

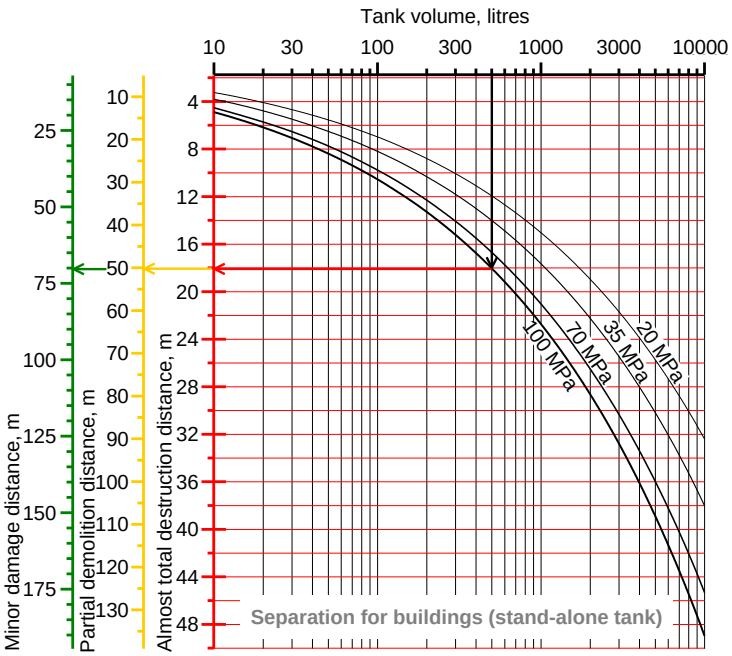

(b)

Figure 29. The nomograms for the determination of hazard distances to humans (a) and to buildings (b) from stand-alone tank rupture.

Rupture of an under-vehicle tank in a fire

Figure 31 shows two nomograms used for the determination of hazard distances for under-vehicle tank rupture in a fire.

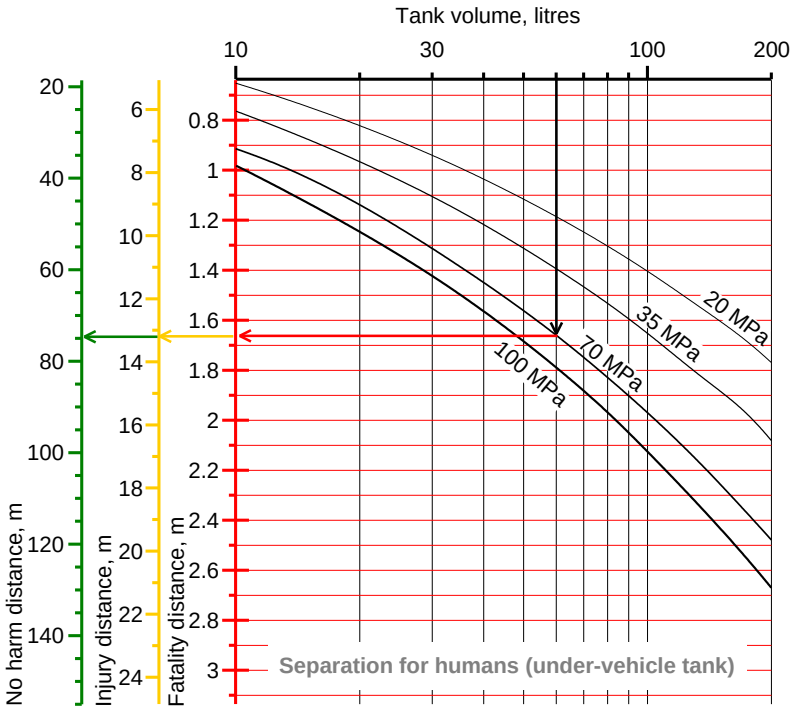

(a)

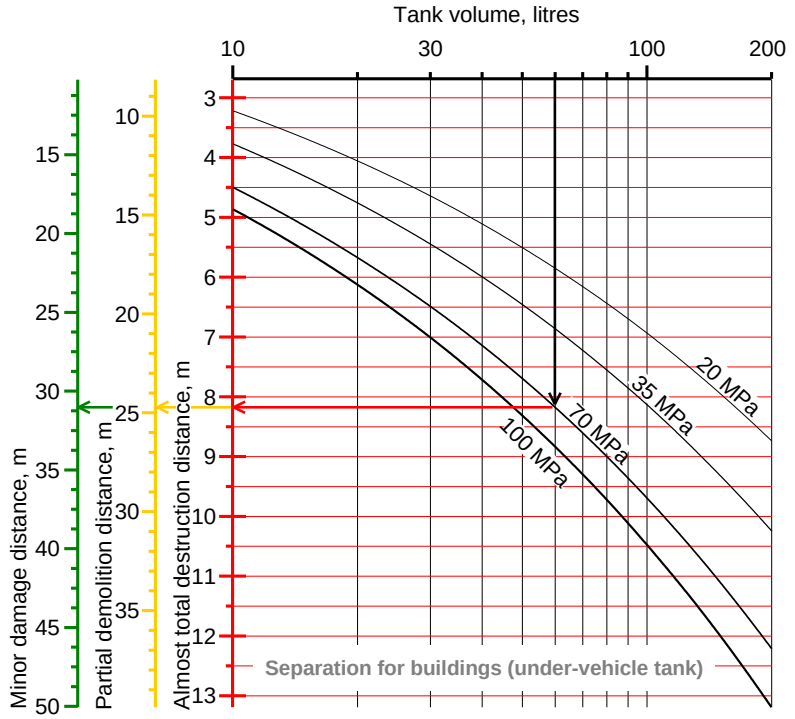

(b)

Figure 30. The nomograms for the determination of hazard distances to humans (a) and to buildings (b) from under-vehicle tank rupture.

Use of the nomograms may be explained graphically with example in Figure 30a. Firstly, the user should select the volume of hydrogen tank on a horizontal axis (e.g. 60 L) and the internal tank pressure on relevant curves (e.g. 70 MPa). The intersection of a pressure curve with the vertical line corresponding to a selected tank volume is shown with a black arrow. Secondly, to find the “fatality” distance, the horizontal line is drawn from the intersection point towards the red vertical axis on the left-hand side (shown with a red arrow). The “fatality” distance equals to 1.67 m in the selected example. To find the “injury” and “no harm” distances,

the line should be simply extended to the yellow and green axes, respectively. In the selected example case, the injury distance is 13.2 m and no harm distance is 75 m.

Effect of missiles and debris

Most modelling approaches deal with the effects of blast and fire. In many hydrogen explosion scenarios however, the throw of missiles or debris is also important and in some cases even dominant. For hydrogen gas explosions this is typically the case for scenarios where some degree of confinement or enclosure is present. When the combustion process changes from a deflagration to a detonation, the throw of missiles or debris can be devastating. Examples include gas explosions inside industrial equipment, inside a garage or car park, or in a nuclear plant. These scenarios may lead to a major hazard of debris or missiles. In these scenarios, it is typically a vessel rupture leading to the throw of missiles. Any risk assessment methodology for hydrogen should contain models for the throw of debris or missiles.

In general, the initial conditions for a throw are defined by the distributions of the missile or debris mass, launch velocity, and launch direction. These conditions are determined by the failure process and the subsequent acceleration by the expanding gasses, or reaction products. This is accompanied by pressure relief as a result of the increasing vent area between the accelerating items.

The break-up process of buildings constructed from reinforced concrete or brick during an internal gas explosion is a more complicated phenomenon. In the case of a (weak) deflagration, the combustion continues during the break-up process and debris launch. The coupling between pressure build-up, venting, and break-up determine which part of the structure will be affected.

Possible prevention and mitigation measures for explosions

Prevention measures [55]:

Passive measures:

- Flow restrictors to minimise hydrogen mass participating in formation of flammable mixture in case of a leak
- Avoid confined spaces if possible
- Natural ventilation
- Absence of ignition sources

Active measures:

- Detection and isolation of hydrogen leaks

Mitigation measures [55]:

Passive measures:

- Deflagration venting
- Hazard and separation distances
- Barriers

Active measures:

- Emergency response
- Detection

- Power shut-down

Mitigation of DDT

Strategies to minimize the potential for flame acceleration or detonation include [43]:

- Avoiding confinement and congestion where flammable hydrogen-air mixtures might form;
- Using flame arrestors, small orifices, or channels to prevent deflagration and detonation from propagating within a system;
- Using diluents, like steam or carbon dioxide, or oxygen depletion techniques where possible and water spray or mist systems to retard flame acceleration. This recommendation of the standard ISO/TR 15916:2004 [43] should be taken with care as hydrogen-air flames are difficult to quench and they can burn or even accelerate around the droplets in heavy sprays of water [59];
- Reduce size of a system where possible to narrow detonability limits;
- Knowing that hydrogen combustion is prone to DDT, especially at large scales, there are serious concerns on how technologies could be made safer. For such kind of applications, the safety strategy could be to organize and control the process of combustion of a hydrogen-contained mixture in a way that the mixture supplied to the burner is between the lower flammability limit and the lower detonability limit.

Prevention of DDT for a fuel cell

Experiments of Pro-Science (Germany) in a mock-up of fuel cell (FC) resulted in the following observations and conclusions:

- A significant flame acceleration was recorded leading to a high overpressure, for the total injected mass of 15 g and 25 g, sufficient for complete demolition of the experimental rig. Both experimental and numerical studies of the FC mock-up suggest that the total injected mass should be less than 6 g for the configuration studied in order to keep overpressures below 10 to 20 kPa. Missile effects could be still possible for this 6 g inventory. Thus, an inventory of 1 g seems a good target for safety for accidental release within this FC mock-up [60].
- The feed line pressure and diameter of a pipe and restrictor orifice should, by design, limit the mass flow rate of hydrogen to a technological level that is required for the FC to function. The release duration, due to the time required to detect the leak and operate the valve should be reduced as much as possible to exclude release of more than 1 g of hydrogen. An estimate shows that for a 50 kW FC, that needs consumption rate of hydrogen just below 1 g/s, a leak detection time and time of shutting down supply line should be together less than 1 s. Any reduction of this time would have a positive impact on safety.
- This last requirement is difficult to achieve for currently available sensors. Innovative systems of leak detection, e.g. based on supply pressure fluctuation analysis, have to be developed and implemented to provide acceptable level of safety. The grid obstacle, used in the Pro-Science experiments to mimic the congestion within real fuel cell, led to strong flame acceleration [60]. The congestion of internal space of the FC enclosure should be avoided as much as possible by a careful design.

Summary

This lecture considered the main features of ‘chemical’ explosions, i.e. deflagrations and detonations, and ‘physical explosions’, i.e. tank ruptures [61]. It discussed overpressures, temperature, flame propagation velocities, etc. of deflagrations and detonations. The hydrogen-air deflagrations in the open atmosphere, in

a closed vessel, and in a tunnel are detailed. DDT and the run-up distance to DDT are covered here as well. The main aspects of vented deflagrations are discussed in this lecture. Detonations, as a worst case scenario, is addressed in the present lecture. Possible prevention and mitigation measures for deflagrations, DDT and denotations are outlined. The evaluation of blast wave effects on humans and structures is carried out with the aid of nomograms.

References

1. Molkov, V (2012). Fundamentals of hydrogen safety engineering, Part I and Part II. Available from: www.bookboon.com, free download e-book.
2. Dorofeev, SB (2007). Evaluation of safety distances related to unconfined hydrogen explosions. International Journal of Hydrogen Energy. Vol. 32, pp. 2118-2124.
3. NFPA, National Fire Protection Association (2009). Compressed Natural Gas (CNG) Vehicular Fuel Systems Code, 52.
4. Chapman, DL (1899). On the rate of explosion in gases. Philosophical Magazine. Vol. 47, pp. 90-104.
5. Jouguet, JCE (1905-1906). On the propagation of chemical reactions in gases. Journal des Mathématiques Pures et Appliquées, vol. 1, pp. 347-425, 1905; continued vol. 2, pp. 5-85, 1906.
6. Alcock, JL, Shirvill, LC and Cracknell, RF (2001). Comparison of existing safety data on hydrogen and comparative fuels. Deliverable report of European FP5 project EIHP2, May 2001. Available from: http://www.eihp.org/public/documents/CompilationExistingSafetyData_on_H2_and_ComparativeFuels_S..pdf [accessed on 13.05.14].
7. Jordan, T (2008). Overview of hydrogen and fuel cell technologies. 1st ISCARW “Progress in Hydrogen Safety”, September 2008, University of Ulster, Belfast
8. Pförtner, H and Schneider, H (1983). Fraunhofer-institut fur treib-und explosivstoffe. ICT-Projektforschung 19/83. Forschungsprogramm "Prozeßgasfreisetzung - Explosion in der Gasfabrik und Auswirkungen von Druckwellen auf das Containment". Ballonversuche zur Untersuchung der Deflagration von Wasserstoff/Luft-Gemischen (Abschlußbericht). Dezember 1983.
9. Molkov, V, Makarov, D and Schneider, H (2006). LES modelling of an unconfined large-scale hydrogen-air deflagration. Journal of Physics D: Applied Physics. Vol. 39, pp. 4366-4376.
10. Molkov, VV, Makarov, DV, Verbecke, F and Schneider, H (2007). Supra LES of accelerating premixed hydrogen-air flames in the open atmosphere. Proceedings of the 3rd International Symposium on Non-Equilibrium Processes, Plasma, Combustion and Atmospheric Phenomena (NEPCAP), Sochi, Russia, June 2007.
11. Gorev, VA, Miroshnikov, SN and Troshin, YaK (1980) Pressure waves from gaseous explosions. In: Detonation, *Proceedings of the VI All-Union Symposium on Combustion and Explosions*, (23-26 September 1980, Almaty), Chernogolovka, Institute of Chemical Physics of Academy of Sciences of USSR, 1980, pp.110-113.
12. Molkov, VV (2009). A multi-phenomena turbulent burning velocity model for large eddy simulation of premixed combustion. *In: Nonequilibrium Phenomena: Plasma, Combustion, Atmosphere*. Eds. Roy GD, Frolov SM and Starik AM, Torus Press, Moscow, pp. 315-323.
13. Verbecke, F, Makarov, D and Molkov, V (2009). VLES of lean hydrogen-air deflagrations in a closed 5.7m height vessel. 6th Mediterranean Combustion Symposium, Ajaccio, France.
14. Kumar, RK and Bowles, EM (1990) Flame acceleration in hydrogen/air mixtures in a vertical cylinder filled with obstacles. Proceedings of the 2nd Int. Conf. on Containment Design and Operation, Toronto, Canadian Nuclear Society, 14-17October 1990.
15. Whitehouse, DR, Greig, DR and Koroll, GW (1996). Combustion of stratified hydrogen-air mixtures in the 10.7 m3 combustion test facility cylinder. Nuclear Engineering and Design. Vol. 166, 453-462.

16. Dorofeev, SB (2008). Flame acceleration and transition to detonation: a framework for estimating potential explosion hazards in hydrogen mixtures. *Lecture presented at the 3rd European Summer School on Hydrogen Safety*, Belfast, UK, 21-30 July 2008.
17. Ciccarelli, G and Dorofeev, S (2008). Flame acceleration and transition to detonation in ducts. Progress in Energy and Combustion Science. Vol. 34, pp. 499–550.
18. Bradley, D (1999). Instabilities and flame speeds in large-scale premixed gaseous explosions. Phil. Trans. R. Soc. Lond. A. Vol. 357, pp. 3567-3581.
19. Bradley, D, Cresswell, TM and Puttock, JS (2001). Flame acceleration due to flame-induced instabilities in large-scale explosions. Combustion and Flame. Vol. 124, pp. 551-559.
20. Lipatnikov, AN (2007). Turbulent combustion of hydrogen-air mixtures. *Lecture presented at the 2nd European Summer School on Hydrogen Safety*, Belfast, UK, 30 Jul – 8 Aug 2007.
21. Lipatnikov, AN and Chomiak, J (2005). Molecular transport effects on turbulent flame propagation and structure. *Progress in Energy and Combustion Science*, vol. 31, pp. 1-73.
22. Kuznetsov, VR and Sabelnikov, VA (1990). Turbulence and Combustion. Hemisphere Publishing Corporation. 1st edition.
23. Groethe, M, Merilo, E, Colton, J, Chiba, S, Sato, Y and Iwabuchi, H (2005). Large-scale hydrogen deflagrations and detonations, *Proceedings of the1st International Conference on Hydrogen Safety*, 8-10 September 2005, Pisa, Paper 120105.
24. Molkov, V, Verbecke, F and Makarov, D (2008). LES of hydrogen-air deflagrations in a 78.5 m tunnel. Combustion Science and Technology. Vol. 180 (5), pp. 796-808.
25. Gamezo, VN, Ogawa, T and Oran, ES (2007). Numerical simulations of flame propagation and DDT in obstructed channels filled with hydrogen-air mixture. Proc. Comb. Inst. Vol. 31, pp. 2463-2471.
26. Landau, LD and Lifshits, EM (1988) Hydrodynamics, Nauka, Moscow, p.733.
27. NFPA 68 (2007) Guide for venting of deflagrations, NFPA, Quincy, MA, USA.
28. Molkov, V, Verbecke, F, and Saffers, JB. (2008). Venting of uniform hydrogen-air deflagrations in enclosures and tunnels: vent sizing and prediction of overpressure. 7th ISHPMIE, St. Petersburg, Russia, July 7–11, 2008.
29. EN14994:2007. Gas explosion venting protective systems.
30. Lamoureux, N, Djebaili-Chaumeix, N and Paillard, C-E (2003). Laminar flame velocity determination for H2-air-He-CO2 mixtures using the spherical bomb. Experimental Thermal and Fluid Science. Vol. 27, pp. 385-393.
31. Tse, SD, Zhu, DL and Law, CK (2000). Morphology and burning rates of expanding spherical flames in H2/O2/inert mixtures up to 60 atmospheres. Proceedings of the 28th Symposium (International) on Combustion, Pittsburgh, PA: The Combustion Institute, pp. 1793-1800.
32. Babkin, VS (2003). Private communication. Institute of Chemical Kinetics and Combustion, Siberian Branch, Russian Academy of Science, Novosibirsk, Russia.
33. Pasman, HL, Groothuizen, ThM and de Gooijer, H (1974). Design of pressure relief vents. *In: Loss Prevention and Safety Promotion in the Process Industries*, Ed. by C.H. Buschman, pp. 185-189.
34. HyIndoor. Deliverable D5.1. "Guidelines on fuel cell indoor installation and use", www.hyindoor.eu
35. Friedrich, A, Grune, J, Jordan, T, Kotchourko, A, Kotchourko, N, Kuznetsov, M, Sempert, K, Stern, G (2007). Experimental study of hydrogen-air deflagrations in flat layer, Intl. Conf. on Hydrogen Safety, 11 – 13 September 2007, San Sebastian, Spain.
36. BRHS, Biennial Report on Hydrogen Safety (2009). The European network of excellence "Safety of hydrogen as an energy carrier" (NoE HySafe). Available from: www.hysafe.org [accessed on 13.05.14].

37. Zbikowski, M, Makarov, D and Molkov, V (2008). LES model of large scale hydrogen–air planar detonations: Verification by the ZND theory. International Journal of Hydrogen Energy. Vol. 33, pp. 4884-4892.
38. Dorofeev, SB, Bezmelnitsin, AV and Sidorov, VP (1995). Transition to detonation in vented hydrogen-air explosions. Combustion and Flame. Vol. 103, pp. 243-246.
39. Tsuruda, T and Hirano, T (1987). Growth of flame front turbulence during flame propagation across an obstacle. *Comb. Sci. Techn*. Vol. 51, pp. 323-328.
40. Pförtner, H and Schneider, H (1984) Final Report for Interatom GmbH, Bergish Gladbach, Germany, October, Fraunhofer ICT Internal Report. (in German).
41. Kuznetsov, M. et al (2005). DDT in a smooth tube filled with a hydrogen-oxygen mixture. Shock Waves. Vol. 14(3), pp. 205-215.
42. NASA (1997). Safety standard for hydrogen and hydrogen systems. Guidelines for hydrogen system design, materials selection, operations, storage, and transportation. Technical report NSS 1740.16, Office of safety and mission assurance, Washington. Available from: http://www.hq.nasa.gov/office/codeq/doctree/canceled/871916.pdf was cancelled on July 25 2005 [accessed 13.05.14].
43. ISO/TR 15916 (2004). Basic considerations for the safety of hydrogen systems. International Organization for Standardization. ISO Technical Committee 197 Hydrogen Technologies. International Organization for Standardization, Geneva.
44. Tieszen, SR, Sherman, MP, Benedick, WB, Shepherd, JE, Knystautas, R and Lee, JHS (1986). Detonation cell size measurements in hydrogen-air-steam mixtures. Progress in Astronautics Aeronautics. Vol. 106, pp. 205–219.
45. Lewis, B and von Elbe, G (1987). Combustion, flames and explosions of gases. 3rd edition. Academic, Press.
46. Breitung, W et al. (2000). Flame acceleration and deflagration-to-detonation transition in nuclear society. NEA/CSNI Report No. NEA/CSNI/R(2000)7.
47. Radulescu, MI, Sharpe, GJ and Law, CK (2005). The Hydrodynamic Structure of Detonations. *Proceedings of the 20th ICDERS*, Montreal, Canada 2005.
48. Bull, DC, Ellworth, JE and Shiff, PJ (1982). Detonation Cell Structures in Fuel/Air Mixtures. Combustion and Flame. Vol. 45(1), pp. 7-22.
49. Lee, JHS (1982). Hydrogen air detonations. *2nd International workshop on the impact of hydrogen on water reactor safety*. Albuquerque, New Mexico.
50. Gavrikov, AI, Efimenko, AA and Dorofeev, SB (2000). A model for detonation cell size prediction from chemical kinetics. Combustion and Flame. Vol. 120, pp. 19-33.
51. Rigas, F and Amyotte, P (2013). Hydrogen safety. Boca Raton: CRC press. Taylor and Francis Group.
52. Cassut, LH (1961). Experimental investigation of detonation in unconfined gaseous hydrogen-oxygen-nitrogen mixtures. ARS Journal. Vol. 31, p.7.
53. Lee, JH, Kynstantus, RC, Guirao, M, Benedick, WA and Shepherd, JE (1982). Hydrogen-Air Detonations. Proceedings of the *2nd International Workshop on the Impact of Hydrogen on Water Reactor Safety*. M. Berman, Ed., SAND82-2456, Sandia National Laboratories, Albuquerque, NM, October.
54. Browne, S and Shepherd, JE (2007). Linear Stability of Detonations with Reversible Chemical Reactions. Extended abstract and work-in-progress poster for the 21rst International Colloquium on the Dynamics of Explosions and Reactive Systems, ENSMA, Poitiers, France, July 22-27, 2007.
55. HyFacts Project. Chapter DM. Hydrogen deflagrations and detonations. Available from: http://hyfacts.eu/category/education-training/ [accessed on 04.01.16].

56. Molkov, V and Kashkarov, S (2015). Blast wave from a high-pressure gas tank rupture in a fire: stand-alone and under-vehicle hydrogen tanks. International Journal of Hydrogen Energy. Vol. 40, no. 36, pp. 12581–12603.
57. Baker, WE, Cox, PA, Westine, PS, Kulesz, JJ and Strehlow, RA (1983). Explosion hazards and evaluation. Elsevier Scientific Publishing Company.
58. Mannan, S (2005). Lees' Loss Prevention in the Process Industries, 3rd ed., vol. 1. Elsevier Butterworth-Heinemann.
59. Shebeko, YuN, Tsarichenko, S G, Eremenko, OYa, Keller, VD and Trunev, AV (1990). Combustion of lean hydrogen-air mixtures in an atomized water stream. Combustion Explosion and Shock Waves. Vol. 26(4), pp. 426-428.
60. Friedrich, A, Kotchourko, N, Stern, G and Veser, A (2009). HYPER experiments on catastrophic hydrogen releases inside a fuel cell enclosure. *Proceedings of the Third International Conference on Hydrogen Safety*, Paper ID 118, 16-18 September 2009, Ajaccio, Corsica, France.
61. Crowl, DA (2003). Understanding explosions.